ACS OMEGA

Open Access

This article is licensed under CC-BY 4.0

http://pubs.acs.org/journal/acsodf

Article

Synthesis and Biological Activity of Iminophosphine Copper(I) Complexes Derived from 2-(Diphenylphosphino)benzaldehyde and 4-Substituted-Benzylamines

Alessio Zavaroni, Luca Rigamonti, Giorgio Pelosi, Lorenzo Verderi, Matteo Incerti, Lisa Menegaldo, Diego Montagner, Dominga Rogolino, Francesca Bonvicini, and Mauro Carcelli*

Cite This: *ACS Omega* 2026, 11, 68833−68845

Read Online

ACCESS | Metrics & More | Article Recommendations | Supporting Information

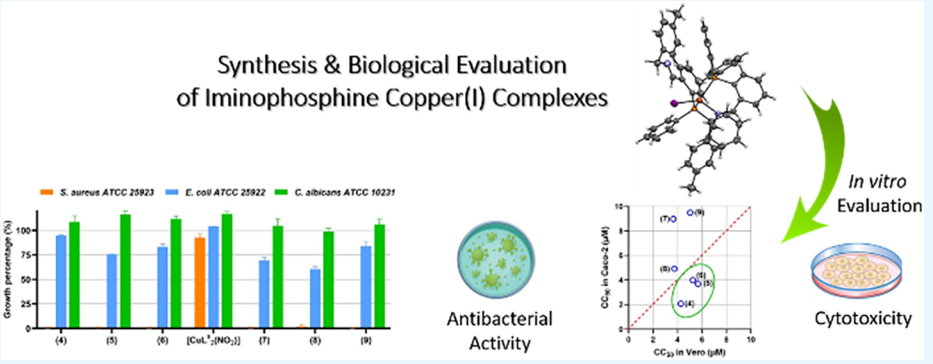

ABSTRACT: A panel of copper(I) complexes was isolated by metal-templated reactions starting from 2-(diphenylphosphino)-benzaldehyde and some 4-substituted-benzylamines, and by changing the ratio between metal and ligand and the anion. The spectroscopic characterization of the copper(I) complexes was completed by discussion of some structures obtained by single-crystal X-ray diffraction. The copper(I) complexes were assayed *in vitro* against *Staphylococcus aureus* ATCC 25923, *Escherichia coli* ATCC 25922, and *Candida albicans* ATCC 10231. Cell viability was assessed both in nonmalignant and malignant cell lines, namely Vero and Caco-2 cells, respectively. While the tested compounds show only a nonspecific antibacterial effect against *S. aureus*, some of them showed an interesting antiproliferative activity.

1. INTRODUCTION

Antimicrobial resistance (AMR) poses a critical threat to global health, as the rapid spread of multidrug-resistant pathogens outpaces the development of traditional antibiotics.[1,2] Metal complexes have re-emerged as a promising therapeutic alternative: unlike conventional drugs, metallo-antimicrobials utilize multitargeted mechanisms and synergistic metal−ligand activities to circumvent resistance.[3] Copper complexes are noteworthy for their multifaced biological activity and their ability to induce cell death via different and often interconnected pathways. These mechanisms include DNA damage, reactive oxygen species (ROS) generation as well as cuproptosis, a recently identified form of regulated cell death occurring in both eukaryotic and prokaryotic cells.[4] This process involves the disruption of copper homeostasis, which targets lipoylated proteins in the tricarboxylic acid cycle and triggers the accumulation of peroxides.[5−7] By disrupting energy metabolism and promoting oxidative stress, these "cuproptosis-like" mechanisms could offer an opportunity for developing a new generation of copper-based antibiotics.[3]

While the anticancer and the antimicrobial activity of copper(II) complexes has been deeply investigated, copper(I) complexes have received much less attention. In fact, copper(I) coordination compounds have been principally studied for their application in catalysis,[8] photochemistry[9] and structural chemistry,[10] while their biological properties are much less investigated. $[Cu(N{-}N)(PR_3)(X)]$ is a class of copper(I) compounds that raised significant interest (X = I^- or NCS^-, N−N = 2,2′-bipyridyl, 1,10-phenanthroline, 2,9-dimethyl-1,10-phenanthroline or 2,2′-biquinoline, PR_3 = tris(aminomethyl)-phosphines).[11] These species have demonstrated notable *in vitro* anticancer activity, and antimicrobial activity against *Staphylococcus aureus* and *Candida albicans*.[11] Recently, a novel class of cationic mixed-ligand copper(I) complexes of type

Received: July 14, 2026
Revised: October 16, 2026
Accepted: October 19, 2026
Published: October 28, 2026



ACS Publications

© 2026 The Authors. Published by American Chemical Society

Downloaded from pubs.acs.org/acsodf/article-pdf/11/44/68833/6900612/acsomega.6c08107.pdf by UNIV DEGLI STUDI DI MODENA user on 17 November 2026

Scheme 1. Schematic Representation of the Iminophosphine Copper(I) Complexes (1)−(9)

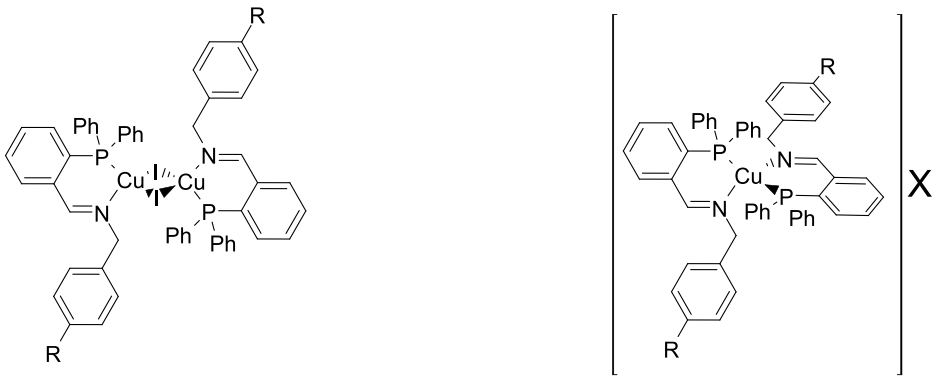

(1) R = H
(2) R = CH_3
(3) R = F

	X = I	X = NO_3^-
R = H	**(4)**	**(7)**
R = CH_3	**(5)**	**(8)**
R = F	**(6)**	**(9)**

Scheme 2. Schematic Representation of the Template Synthesis of the Copper(I) Complexes (1)−(3). Reagents and Conditions: (1) 1/1 MeCN/$CHCl_3$, 50 °C, N_2, 1 h; (2) MeCN, 65 °C, N_2, 5 h

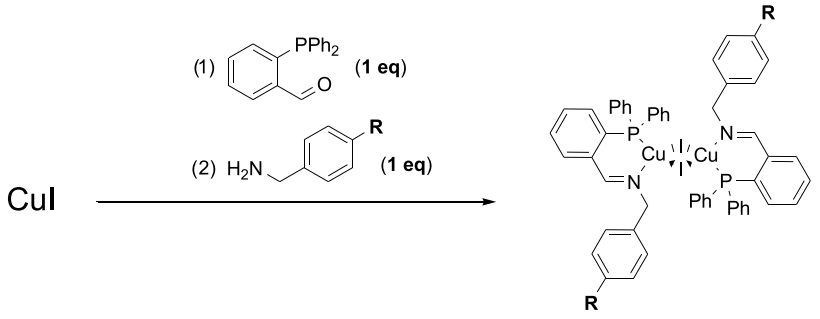

(1) R = H
(2) R = Me
(3) R = F

$[Cu(N)(P)_2]^+$ was disclosed, where N is a phenoxy-ketimine and P is a monodentate tertiary phosphine. These compounds proved to be active against the Gram-positive *S. aureus* and the Gram-negative *E. coli*.[12] Some metal(I)-NHC carbene complexes have been also investigated for their antibacterial activity (NHC, N-heterocyclic carbene, metal = Ag, Cu, or Au): Ag(I) and Cu(I) complexes resulted the most efficient at inhibiting biofilm formation.[13,14]

To the best of our knowledge, no biological data are available for copper(I) complexes with P,N ligands, particularly iminophosphines. These organic molecules have been extensively used for the synthesis of complexes with gold and palladium,[15−17] while few iminophosphine copper(I) complexes are reported in literature.[18,19] Here, a synthetic strategy based on template reactions starting from 2-(diphenylphosphino)benzaldehyde and some 4-substituted-benzylamines allowed to prepare the copper(I) iminophosphine complexes **(1)−(9)** by varying the metal to ligand *ratio* (1:1 or 1:2) and the nature of the counteranion (Scheme 1).

The complexes **(4)−(9)**, stable in the assay conditions, were tested *in vitro* against *S. aureus* ATCC 25923, *E. coli* ATCC 25922, and *C. albicans* ATCC 10231, chosen as representative of Gram positive, Gram negative and fungal microorganisms, respectively. Cytotoxicity in malignant Caco-2 cell line was also investigated, and the obtained CC_{50} values were compared to those measured in Vero cells to individuate compounds with anticancer potential.

2. RESULTS AND DISCUSSION

2.1. Synthesis and Characterization of Iminophosphine Copper(I) Complexes

We started to synthesize some copper(I) complexes with 2-(diphenylphosphino)benzaldehyde (PCHO) and with some imine ligands obtained from it, aiming to investigate their antimicrobial and cytotoxic properties. The isolation of the product of the reaction between PCHO and arilamines could be tedious and resulting in poor yields. After several attempts, for example, we obtain N-[2-(diphenylphosphino)-

https://doi.org/10.1021/acsomega.6c08107
ACS Omega 2026, 11, 68833−68845

Downloaded from pubs.acs.org/acsodf/article-pdf/11/44/68833/6900612/acsomega.6c08107.pdf by UNIV DEGLI STUDI DI MODENA user on 17 November 2026

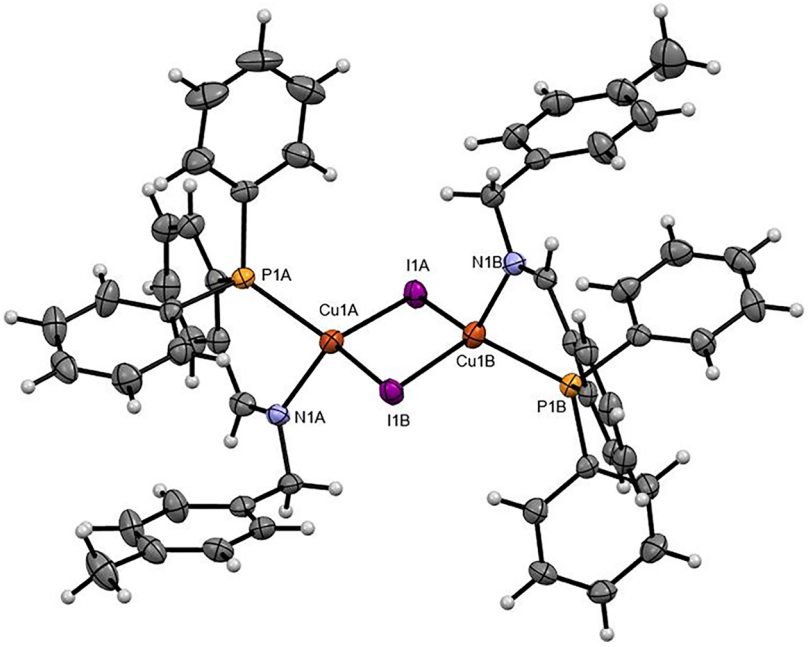

Figure 1. ORTEP diagram of the crystal structure of the complex (**2**), drawn with 50% probability ellipsoids (phosphorus atoms in light orange, nitrogen in blue, carbon in gray, hydrogens in white, iodine in purple, copper in dark orange).

Scheme 3. Template Synthesis of the Complexes (4)−(6)[a]

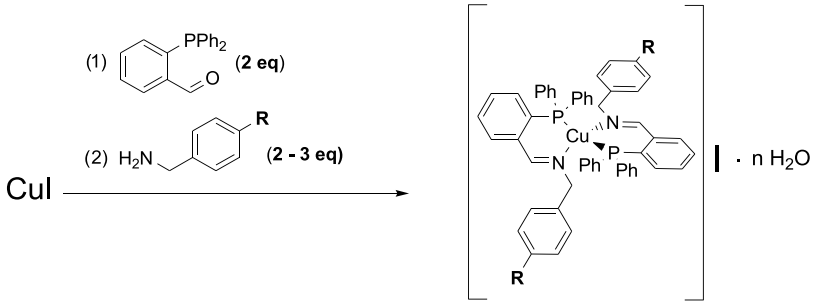

(4) R = H, n = 0
(5) R = Me, n = 2
(6) R = F, n = 4

[a]Reagents and conditions: (1) 1/1 MeCN/$CHCl_3$, 50 °C, N_2, 1 h; (2) MeCN, 65 °C, N_2, 5 h.

benzylidene]benzylamine L^1 with a yield of about 21%. To circumvent synthetic problems, the copper(I) complexes (**1**)−(**9**) were directly obtained through template reactions. First, copper(I) iodide was reacted with PCHO and the proper amine (benzylamine, 4-methyl or 4-fluorobenzylamine) in 1:1:1 stoichiometric ratio in acetonitrile/chloroform mixture under inert atmosphere, affording the complexes (**1**)−(**3**) (Scheme 2).

The formation of the imine bond was confirmed by IR spectroscopy (appearance of a band at about 1628 cm^{-1} and disappearing of the C═O stretching band of the PCHO reagent, Figures S1−S3). Red-orange single crystals suitable for XRD analysis were obtained by slow evaporation of a solution of (**2**) in $CHCl_3$. The crystal data revealed a dimeric structure $[Cu(\mu\text{-}I)L^n]_2$ with each copper(I) ion coordinated to the P,N-bidentate iminophosphine ligand L^n and two iodine atoms (Figure 1 and Figure S4). The iodine atoms bind to the metal centers in a bridging mode, and the phosphorus and nitrogen atoms of the two coordinated ligands adopt a *trans* configuration. The bite angles of the ligands, P1A-Cu1A-N1A and P1B−Cu1B-N1B, are 88.95° and the coordination geometry of copper(I) is distorted tetrahedral. The Cu1A-Cu1B distance is 2.930 Å, higher than the sum of the van der Waals radii of two copper atoms (2.80 Å), and this excludes any significant metallophilic interaction.

Single crystal XRD analysis allowed to confirm that (**1**) and (**3**) have the same structure of (**2**); Figure S5 shows the crystal structures of (**3**) and its crystallographic characterization, while (**1**) was previously reported.[20]

As expected, (**1**)-(**3**) exhibit similar behavior in solution (Figures S6−S9). In the spectra of the complex (**1**), for example, both the phosphorus and the imine proton resonances experiment a significant shielding with respect to the free ligand L^1 (Figure S6a,b). The complexes (**1**)-(**3**) are stable in $CDCl_3$ solution over 3 days, while in a coordinating solvent like DMSO-d_6, more than one set of signals can be found in the ^1H NMR spectra immediately after dissolution. After 1 day a peak at 28.77 ppm, attributable to a phosphine

https://doi.org/10.1021/acsomega.6c08107
ACS Omega 2026, 11, 68833−68845

Downloaded from pubs.acs.org/acsodf/article-pdf/11/44/68833/6900612/acsomega.6c08107.pdf by UNIV DEGLI STUDI DI MODENA user on 17 November 2026

oxide, appeared in the ^{31}P NMR spectrum (Figure S6c). ESI-MS analyses confirmed the presence of the $[CuL]^+$ species in solution (Figures S10−S12).

The 1:1 complex $[Cu(\mu\text{-I})(MeCN)L^a]_2$ (L^a = PCHO) was also isolated and characterized (Figures S13−S17) as reported in the literature.[21] The formation of the complex was supported by IR and NMR spectroscopy, where it is evident the shift of the C═O signal respect to the free aldehyde (Figures S13−S15), and by ESI-MS analysis (Figure S16). Figure S17 reports the comparison between experimental powder diffractogram of complex $[Cu(\mu\text{-I})(MeCN)L^a]_2$ and the calculated one obtained from literature data,[21] confirming the structure of the complex.

The synthesis of the 2:1 iminophosphine:copper(I) complexes (**4**)−(**6**) was carried out as shown in Scheme 3. An excess of aldehyde and 4-fluorobenzylamine amine reagents (up to 3 equiv.) is required to obtain (**6**), otherwise the previously characterized 1:1 species (**3**) was isolated.

The FT-IR spectra of the complexes (**4**)-(**6**) are similar to the spectra of the corresponding 1:1 ones, with the iminic stretching band at about 1626 cm^{-1} (Figures S18−S20). In the ^{31}P NMR spectra of (**4**)-(**6**) there is a single peak, confirming the symmetry of the complexes with the ligands behaving as P,N bidentate (Scheme 3). The presence of only one set of signals for the ligand backbone in their ^{1}H NMR spectra also supports this hypothesis. It is interesting to note that (**4**) is soluble in acetonitrile, chloroform and DMSO, contrarily to the dimeric complex (**1**) with the same ligand L^1. The ^{1}H and ^{31}P NMR spectra of (**4**) in $CDCl_3$, compared with the spectra of (**1**) and L^1, are shown in Figure S21. The complex (**4**) is stable in $CDCl_3$ solution over 1 week, with only traces of formation of phosphine oxide (Figure S22). Contrarily to the 1:1 complexes, (**4**) - (**6**) are stable also in DMSO-d_6 (Figures S23−S28). ESI-MS analyses confirmed the presence of $[CuL_2]^+$ species in solution (Figures S29−S31).

After precipitation of the complex (**5**), slow evaporation of the mother liquors afforded some crystals that, quite surprisingly, were characterized by XRD as the new product (**5a**) (Figure 2 and Figure S32).

In the complex (**5a**), one ligand acts as P,N-bidentate and the other in P-monodentate fashion; iodide completes the coordination sphere of the copper(I) ion. The bite angle of the bidentate ligand is 88.38°, while the other coordination angles are larger than 100° giving rise to a distorted tetrahedron. The distance Cu−I is 2.681 Å, the bond lengths of the biting atoms are Cu−N 2.164 and Cu−P 2.306 Å, while the one with the monodentate ligand is consistently Cu−P 2.305 Å.

The complex $[Cu(L^a)_2I]$ (L^a = PCHO; Experimental part and Figures S33−S35) with a 2:1 ligand:metal stoichiometry was also isolated and characterized.

We also explored the synthesis of the copper(I) complexes (**7**)-(**9**) with nitrate as counterion (Scheme 4). They were prepared *via* a comproportionation reaction between copper-(II) nitrate and metallic copper in acetonitrile. $[Cu(MeCN)_4]$-NO_3 was produced *in situ* and immediately consumed in the template synthesis.[22]

The presence of only one strong band in the FT-IR spectrum in the range 1400 − 1300 cm^{-1} (Section 3 and Figures S36−38) suggests that the complexes (**7**)−(**9**) are ionic in the solid state.[23] Single crystals of (**7**) suitable for XRD were obtained via slow evaporation of the mother liquor (Figure 3 and Figure S46). In agreement with the IR spectroscopic data, the crystal structure reveals an ionic framework of type $[Cu(L^1)_2]NO_3$ with a distorted tetrahedral geometry around the copper(I) center; the imine group of one of the two P,N-bidentate ligands is disordered within the crystal lattice.

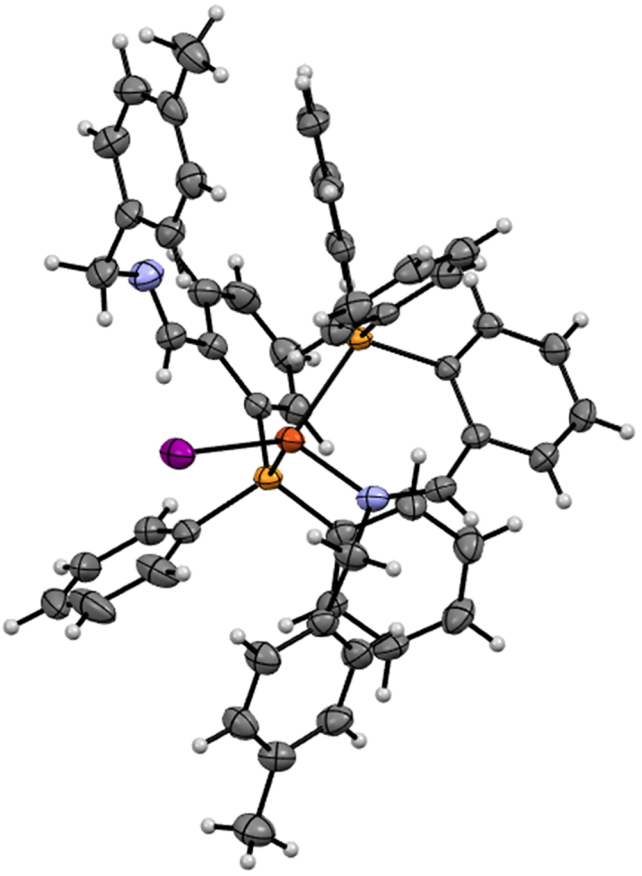

Figure 2. ORTEP diagram of the crystal structure of (**5a**), drawn with 50% probability ellipsoids (phosphorus atoms in light orange, nitrogen in blue, carbon in gray, hydrogens in white, iodine in purple, copper in dark orange).

As an example, Figure S39 reports the ^{31}P and ^{1}H NMR of complex (**7**). The complexes (**7**)−(**9**) are stable in DMSO-d_6 for over 1 week, with no detectable formation of phosphine oxide species (Figure S40−44). ESI-MS spectra are reported as Figure S45.

Finally, the complex $[\mathbf{CuL_2^a(NO_3)}]$ (Figures S47−50) was isolated and characterized. The FT-IR spectrum shows two strong bands at 1434 and 1286 cm^{-1} ascribable to the N−O stretching of the nitrate group coordinated to the metal center.[24] Single crystal X-ray diffraction analysis confirmed that the nitrate anion is bidentate, while the two ligands act as P-monodentate (Figure S48). The coordination geometry around the copper(I) center is a distorted tetrahedron.

2.2. Biological Evaluation

The copper(I) iminophosphine complexes (**4**)−(**9**) and $[\mathbf{CuL_2^a(NO_3)}]$, stable and soluble in the testing medium, were assayed *in vitro* against *S. aureus* ATCC 25923, *E. coli* ATCC 25922, and *C. albicans* ATCC 10231. These strains were selected as representative Gram-positive, Gram-negative and fungal microorganisms, respectively, commonly used in studies aimed at evaluating the antimicrobial activity of newly synthesized compounds and other potentially bioactive agents,[24,25] including copper-based antimicrobials.[26]

Downloaded from pubs.acs.org/acsodf/article-pdf/11/44/68833/6900612/acsomega.6c08107.pdf by UNIV DEGLI STUDI DI MODENA user on 17 November 2026

https://doi.org/10.1021/acsomega.6c08107
ACS Omega 2026, 11, 68833−68845

Scheme 4. Template Synthesis of the Complexes (7)−(9)[a]

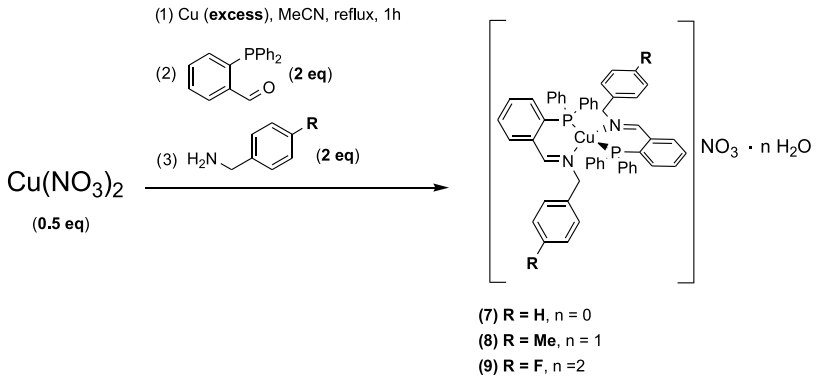

[a]Reagents and conditions: (1) 1/1 MeCN/$CHCl_3$, 50 °C, N_2, 1 h; (2) MeCN, 65 °C, N_2, 5 h.

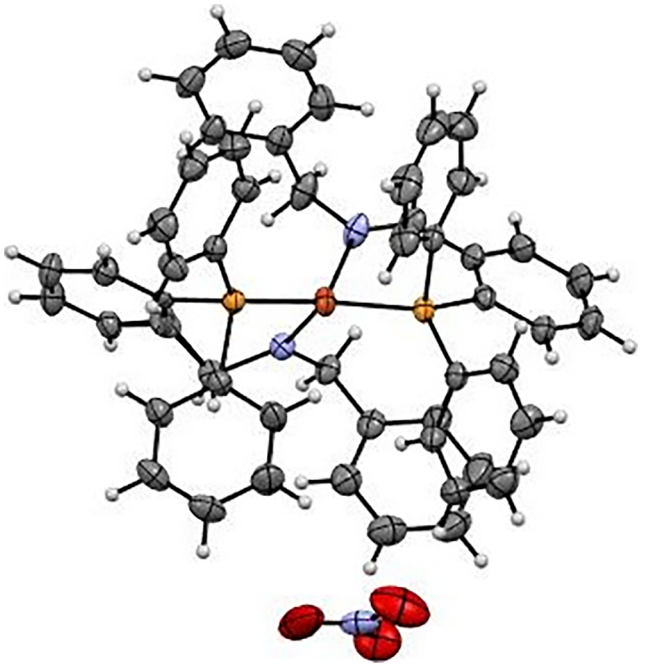

Figure 3. ORTEP diagram of the crystal structure of (7), drawn with 50% probability ellipsoids (phosphorus atoms in light orange, carbon in gray, hydrogens in white, nitrogen in blue, oxygen in red, copper in dark orange). Only one ligand position (occupancy 50%) is represented.

The activity of the metal complexes was initially evaluated at a concentration of 100 μM against the three selected microbial species to obtain a preliminary overview of their antimicrobial potential (Figure 4).

Based on these results, both iodide- and nitrate-containing complexes appeared to strongly inhibit the growth of *S. aureus*, while $[\mathbf{CuL_2^a(NO_3)}]$ did not interfere with microbial proliferation. In contrast, none of them exhibited antifungal properties against *C. albicans* as fungal growth remained close to 100% in all cases. Regarding *E. coli*, growth percentages ranged from 60.4% (**8**) to 104.1% (**6**), however none of the compounds could be considered biologically active against this Gram-negative strain. These differences in susceptibility may be attributed to variations in the cell envelope architecture of the tested species, which constitute distinct permeability barriers and may therefore lead to divergent physicochemical requirements for compounds to exert inhibitory activity against each microbial species.

The panel of metal compounds (**4**)−(**9**) were subjected to dose−response experiments to determine their IC_{50} (half maximal inhibitory concentration) values against *S. aureus* together with their CC_{50} (50% cytotoxic concentration) values in the Vero cell line (Figure 5), leaving aside the inactive $[\mathbf{CuL_2^a(NO_3)}]$. These values were also determined for the reference drugs serving as internal controls in the biological assays (Table S51). These cells, which represent a non-malignant mammalian cell model, are internationally recommended as a standard system for assessing the cytotoxicity of pure compounds as well as a wide range of products and formulations (ISO 10993−5). Under our experimental

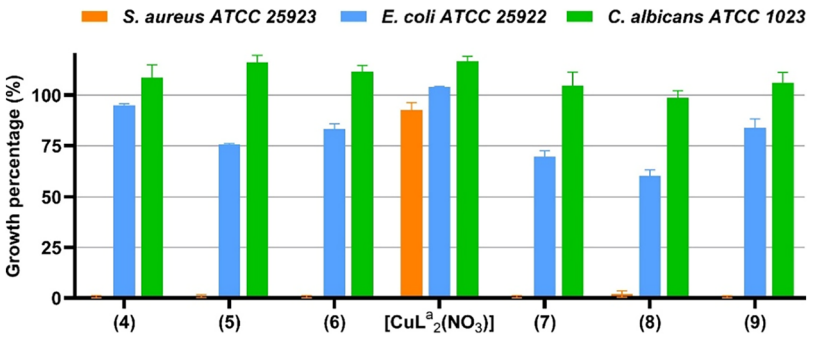

Figure 4. Screening of the antimicrobial activity of copper(I) iminophosphine complexes (**4**)−(**9**) and $[\mathbf{CuL_2^a(NO_3)}]$ at 100 μM. Results are expressed as percentage of microbial growth relative to untreated controls (100%). Data represent mean values ± standard deviation.

https://doi.org/10.1021/acsomega.6c08107
ACS Omega 2026, 11, 68833−68845

Downloaded from pubs.acs.org/acsodf/article-pdf/11/44/68833/6900612/acsomega.6c08107.pdf by UNIV DEGLI STUDI DI MODENA user on 17 November 2026

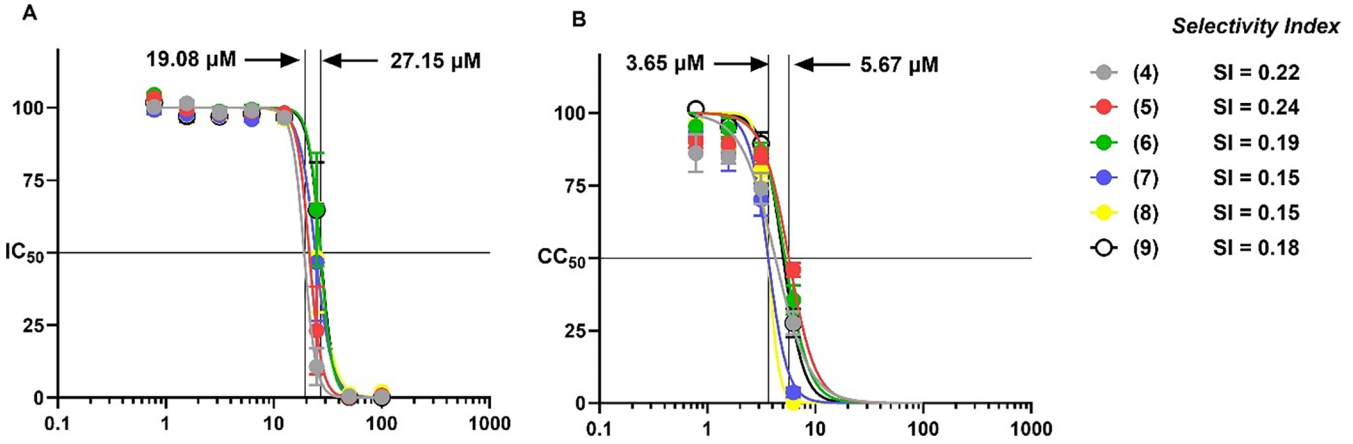

Figure 5. Dose−response curves of the complexes showing (A) antibacterial activity against *S. aureus* and (B) cytotoxicity in Vero cells. Data are expressed as percentage of growth inhibition (A) or cell viability (B) relative to untreated controls and are plotted as a function of the logarithm of compound concentration (μM). IC_{50} and CC_{50} values are indicated by the intersection with the 50% response level. The selectivity index (SI), calculated as CC_{50}/IC_{50}, is reported for each compound, highlighting their limited selectivity toward bacterial cells over mammalian cells.

conditions, the IC_{50} values for *S. aureus* ranged from 19.08 to 27.15 μM (Table S52), whereas the CC_{50} values for Vero cells ranged from 3.52 to 5.67 μM (Table S53), confirming the well-known toxicity of some metal-based compounds.[27,28] The current iminophosphine substituents imparted minimal variations in bioactivity; expanding this scaffold with groups of contrasting lipophilicity and electronic character will be necessary to establish reliable SAR rules.

The obtained results indicate that the synthesized copper(I) iminophosphine complexes are more cytotoxic toward mammalian cells than effective against *S. aureus*, as reflected by the selectivity index (SI) values lower than 1. Overall, this profile suggests a lack of selectivity and points to a nonspecific antibacterial effect.

This consideration prompted us to further investigate the biological profile of the copper(I) iminophosphine complexes in a different cellular context, namely the human colorectal adenocarcinoma-derived epithelial Caco-2 cells, thereby extending the evaluation beyond nonmalignant models. Thus, dose−response curves were generated in Caco-2 cells (Figure S54, Table S55) and the obtained CC_{50} values were compared to those measured in Vero cells (Figure 6). Such comparative analysis identifies three compounds, (**4**), (**5**) and (**6**), as possible candidates with an anticancer potential. Differences in cytotoxic potency could be attributed to the counterion, which dictates the complex ionic status, overall lipophilicity, and, probably, efficiency of cellular uptake.

The biological properties of the compounds were further explored using human red blood cells (hRBCs), which serve as a well-established model for evaluating interactions with biological membranes and for assessing preliminary systemic safety in view of potential therapeutic applications. Notably, none of the copper(I) iminophosphine complexes exhibited significant hemolytic activity at their antiproliferative concentrations (Table S55), suggesting that their biological effect is not associated with nonspecific membrane disruption (Figure 7). Rather, the absence of significant membrane damaging is consistent with the involvement of an intracellular mechanism of action. Such intracellular effects may arise from different molecular pathways.

When a plasmid DNA interaction assay was performed under cell-free conditions, a clear ability to induce damage to

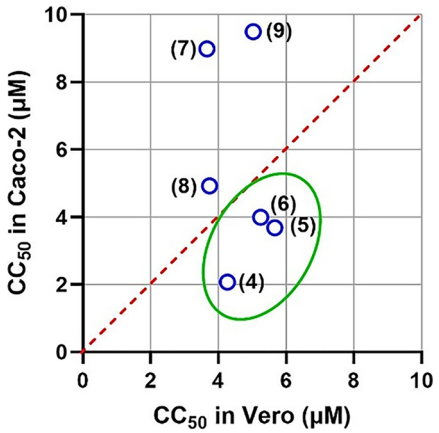

Figure 6. Correlation between CC_{50} values determined in Caco-2 and Vero cells. Each blue circle represents a copper(I) iminophosphine complex. The red line corresponds to the equality (CC_{50} Caco-2 = CC_{50} Vero). Compounds located below the line exhibit lower CC_{50} values in Caco-2 cells compared to Vero cells, indicating a higher cytotoxicity toward cancer cells and, therefore potential antiproliferative activity. Compounds above the line are more cytotoxic toward nonmalignant cells, suggesting lower selectivity for cancer cells. The green ellipse highlights the compounds that showed antiproliferative activity on Caco-2 cells.

plasmid DNA was observed although with different efficiencies (Figure 8). (**4**) and (**8**) showed a strong nuclease effect, with a significant loss of detectable DNA bands, suggesting extensive DNA fragmentation and/or degradation. (**5**), (**6**) and (**7**) exhibited weaker activity, with less pronounced DNA degradation, while [$\mathbf{CuL_2^a(NO_3)}$] and (**9**) did not significantly interact with the plasmid DNA. The changes in the electrophoretic pattern of the plasmid are consistent with an interaction with DNA and, for some complexes (**4**) and (**8**), with substantial DNA damage. This nuclease activity may contribute to the observed reduction in proliferation of both *S. aureus* and mammalian cells. However, alternative mechanisms of action may also contribute to the biological effects observed in these cellular systems, including cuproptosis. Further investigations are therefore warranted to elucidate the molecular pathways underlying the biological activity of these

Downloaded from pubs.acs.org/acsodf/article-pdf/11/44/68833/6900612/acsomega.6c08107.pdf by UNIV DEGLI STUDI DI MODENA user on 17 November 2026

https://doi.org/10.1021/acsomega.6c08107
ACS Omega 2026, 11, 68833−68845

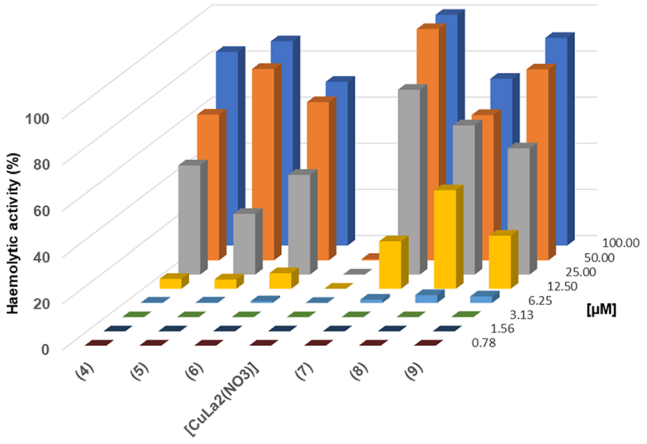

Figure 7. Hemolytic activity of copper(I) iminophosphine complexes evaluated on hRBCs. Hemolysis is expressed as mean percentage values relative to the positive control (1% Triton X-100, 100% hemolysis), with untreated cells in PBS as the negative control (0% hemolysis).

complexes and to assess their potential for therapeutic applications.

3. EXPERIMENTAL SECTION

3.1. Chemistry

Commercial reagents were purchased from Sigma-Aldrich. The purity of the synthesized compounds was determined by elemental analysis and verified to be ≥ 95%. ^{1}H, ^{13}C and ^{31}P and NMR spectra were recorded at 25 °C on a Bruker Advance 400 MHz FT spectrometer or on a Bruker Advance 500 MHz FT spectrometer. The ATR-IR spectra were recorded by means of a PerkinElmer spectrophotometer by using a diamond crystal plate in the range of 4000−400 cm^{-1}. Elemental analyses were performed by using a Thermo Fisher FlashSmart CHNS/O analyzer with gas-chromatographic separation. Electrospray ionization mass spectral analyses (ESI-MS) were performed with an ESI time-of-flight Micromass 4LCZ spectrometer. Samples were dissolved in methanol or acetonitrile. Powder X-ray diffraction (P-XRD) data were collected with a Rigaku Smartlab XE diffractometer equipped with a 2D HyPix3000 detector operating in 1D mode. Data were collected under ambient conditions in Bragg−Brentano geometry (Cu Kα λ = 1.5046 Å) in continuous mode, in the 2−50° 2θ angular range, with a step size of 0.01° at a scan speed of 8° min^{-1}.

3.1.1. *N*-(2-(Diphenylphosphino)phenyl)-methylene Benzylamine (L^{1}). Benzylamine (49 μL, 0.447 mmol, 1.3 equiv) was added to a yellow solution of PCHO (100 mg, 0.344 mmol, 1.0 equiv) in 3/1 MeOH/DCM (9 mL/3 mL) mixture; the resulting solution was stirred under reflux overnight. The obtained colorless solution was allowed to cool to RT, then it was reduced to a small volume (ca. 1−2 mL) and left at −20 °C overnight. A white precipitate formed, which was filtered, washed with a small volume of cold MeOH and dried *in vacuo*. **L^{1}** was isolated as a white solid (28 mg, yield = 21%). IR (cm^{-1}): ν = 3052 (w) (CH sp^{2}), 2829 (w) (CH sp^{3}), 1636 (m) (C═N). ^{1}H NMR (400 MHz, $CDCl_3$, 298 K): δ(ppm) = 9.04 (d, J = 5.1 Hz, 1H, CH═N), 8.07 (ddd, J = 7.8, 4.0, 1.4 Hz, 1H, ArH), 7.44−7.27 (m, 13H, ArH), 7.25−7.21 (m, 2H, ArH), 7.08−7.02 (m, 2H, ArH), 6.93−6.86 (m, 1H, ArH), 4.70 (s, 2H, CH_2). ^{1}H NMR (400 MHz, DMSO-d_6, 298 K): δ(ppm) = 8.93 (d, J = 4.8 Hz, 1H, CH═N), 7.95 (ddd, J = 7.6, 4.0, 1.5 Hz, 1H, ArH), 7.50−7.36 (m, 8H, ArH), 7.26−7.17 (m, 7H, ArH), 7.02−6.94 (m, 2H, ArH), 6.82 (ddd, J = 7.7, 4.5, 1.4 Hz, 1H, ArH), 4.62 (s, 2H, CH_2). ^{13}C NMR (101 MHz, $CDCl_3$, 298 K): δ(ppm) = 160.71 (d, J = 22.5 Hz), 139.50 (d, J = 17.3 Hz), 139.08, 137.77, 137.58, 136.45 (d, J = 9.5 Hz), 134.23 (d, J = 20.0 Hz), 133.35, 132.12, 130.53, 129.07, 129.04, 128.84, 128.77, 128.50, 128.15, 127.81 (d, J = 4.4 Hz), 126.93, 65.23. ^{31}P NMR (162 MHz, $CDCl_3$, 298 K): δ(ppm) = −14.01 (s). ^{31}P NMR (162 MHz, DMSO-d_6, 298 K): δ(ppm) = −14.49 (s). MS-ESI (positive ions; MeOH): m/z (%): 275 (100) [M−C_7H_6N]$^{+}$, 380 (98) [M + H]$^{+}$. Elem. anal. calcd (%) for $C_{26}H_{22}NP$: C 82.30%, H 5.84%, N 3.69%; found: C 82.06%, H 5.79%, N 3.41%.

3.1.2. General Procedure for the Synthesis of 1:1 Iminophosphine:Copper(I) Complexes. The reaction was performed under N_2 atmosphere, and the solvents were degassed prior to use. To a solution of PCHO (100 mg, 0.344 mmol, 1.0 equiv) in $CHCl_3$ (10 mL) was added a solution of CuI (65.9 mg, 0.346 mmol, 1.0 equiv) in MeCN (10 mL) and the resulting mixture was stirred at 50 °C for 1 h (after 15 min a yellow precipitate formed). The desired amine (0.344 mmol, 1.0 equiv) in MeCN (10 mL) was added and the resulting suspension was stirred at 60−65 °C for 5 h: the initial yellow suspension became an orange-red solution and then an orange precipitate formed. The mixture was allowed to cool to RT, then it was left at 4 °C under nitrogen overnight. The precipitate was filtrated, washed with cold MeCN and dried *in vacuo*.

3.1.2.1. [Cu(μ-I)L^{1}]$_2$ (1). Benzylamine (37.6 μL, 0.344 mmol) was used for the synthesis. The product was isolated as an orange-red powder (75 mg, yield = 38%). Mp 245−248 °C (dec.). IR (cm^{-1}): ν

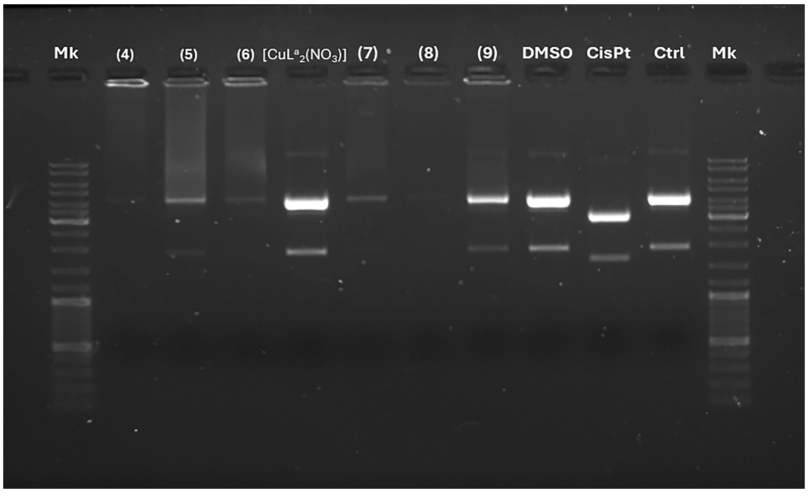

Figure 8. Agarose gel electrophoresis analysis of pmaxGFP (3527 bp) with the metal complexes at 100 μM. Mk: molecular weight marker (Gene Ruler DNA ladder mix); DMSO: solvent control; Ctrl: plasmid DNA control; CisPt (cisplatin) with a different pattern, consistent with its known mechanism to form covalent Pt-DNA adducts and cross-links.

Downloaded from pubs.acs.org/acsodf/article-pdf/11/44/68833/6900612/acsomega.6c08107.pdf by UNIV DEGLI STUDI DI MODENA user on 17 November 2026

https://doi.org/10.1021/acsomega.6c08107
ACS Omega 2026, 11, 68833−68845

= 3033 (w) (CH sp^2), 2842 (w) (CH sp^3), 1628 (m) (C═N). ^{1}H NMR (400 MHz, $CDCl_3$, 298 K): δ(ppm) = 8.15 (s, br, 2H, CH═N), 7.59−7.26 (m, 24H, ArH), 7.25 (s, 2H, ArH), 7.22−6.85 (m, 12H, ArH), 5.02 (s, br, 4H, CH_2). ^{31}P NMR (162 MHz, $CDCl_3$, 298 K): δ(ppm) = −16.13 (s, br). MS-ESI (positive ions; MeCN): m/z (%): 442 $[CuL^1]^+$. Elem. anal. calcd (%) for $C_{52}H_{44}Cu_2I_2N_2P_2$: C 54.80%, H 3.89%, N 2.46%; found: C 54.76%, H 3.84%, N 2.42%. Single crystals suitable for XRD analysis were obtained by slow evaporation of a solution of the complex in $CHCl_3$.

3.1.2.2. [Cu(μ-I)L^2]$_2$ ***(2).*** After the addition of 4-methylbenzylamine (43.8 μL, 0.344 mmol), temperature was raised to 60 °C. The product was isolated as an orange-red powder (99 mg, yield = 49%). Mp 190−192 °C (decomp.). IR (cm^{-1}): ν = 3046 (w) (CH sp^2), 2845 (w) (CH sp^3), 1627 (m) (C═N). ^{1}H NMR (400 MHz, $CDCl_3$, 298 K): δ(ppm) = 8.13 (s, br, 2H, CH═N), 7.60−7.27 (m, 24H, ArH), 7.25 (s, 2H, ArH), 6.99 (m, 10H, ArH), 4.98 (s, br, 4H, CH_2), 2.28 (s, 6H, CH_3). ^{31}P NMR (162 MHz, $CDCl_3$chloroform-*d*, 298 K): δ(ppm) = −15.72 (s, br). MS-ESI (positive ions; MeCN): m/z (%): 456 (100) $[CuL^2]^+$, 850 (25) $[CuL_2^2]^+$. Elem. anal. calcd (%) for $C_{54}H_{48}Cu_2I_2N_2P_2$: C 55.54%, H 4.14%, N 2.40%; found: C 55.65%, H 4.07%, N 2.34%. Single crystals suitable for XRD analysis were obtained by slow evaporation of mother liquors.

3.1.2.3. [Cu(μ-I)L^3]$_2$ ***(3).*** After the addition of the 4-fluorobenzylamine (39.3 μL, 0.344 mmol) amine, temperature was raised to 65 °C. The product was isolated as an orange-red powder (151 mg, yield = 71%). Mp 245−248 °C (dec.). IR (cm^{-1}): ν = 3046 (w) (CH sp^2), 2841 (w) (CH sp^3), 1628 (m) (C═N). ^{1}H NMR (400 MHz, $CDCl_3$, 298 K): δ(ppm) = 8.16 (s, br, 2H, CH═N), 7.59−7.26 (m, 26H, ArH), 7.06−6.98 (m, 6H, ArH), 6.78 (t, J = 8.5 Hz, 4H, ArH), 4.96 (s, br, 4H, CH_2). ^{31}P NMR (162 MHz, $CDCl_3$, 298 K): δ(ppm) = −15.77 (s, br). MS-ESI (positive ions; MeCN): m/z (%): 460 (100) $[CuL^3]^+$, 857 (40) $[CuL_2^3]^+$. Elem. anal. calcd (%) for $C_{52}H_{42}Cu_2F_2I_2N_2P_2$: C 53.12%, H 3.60%, N 2.38%; found: C 53.25%, H 3.62%, N 2.34%. Single crystals suitable for XRD analysis were obtained by slow evaporation of mother liquors.

3.1.3. General Procedure for the Synthesis of 2:1 Iminophosphine:Copper(I) Complexes Derived from CuI. The reaction was performed under N_2 atmosphere and the solvents were degassed prior to use. To a solution of PCHO (100 mg, 0.344 mmol, 2.0 equiv) in $CHCl_3$ (10 mL) was added a solution of CuI (32.8 mg, 0.172 mmol, 1.0 equiv) in MeCN (10 mL) and the resulting mixture was stirred at 50 °C for 1 h (after 15−20 min a yellow precipitate formed). The desired amine (0.344 mmol, 2.0 equiv) in MeCN (10 mL) was added and the resulting suspension was stirred at 50 °C for 5 h: the initial yellow suspension became a bright orange-red solution. The solution was allowed to cool to RT, then, depending on the amine, it was reduced to a small volume (3−4 mL) and an appropriate antisolvent was added, otherwise it was dried and recrystallized with the proper solvent mixture. The resulting precipitate was filtrated, washed with the appropriate solvent and dried *in vacuo*.

3.1.3.1. Cu(L^1)$_2$I ***(4).*** Benzylamine (37.6 μL, 0.344 mmol) was used for the synthesis. Et_2O was used as antisolvent. The product was isolated as a light orange solid (98 mg, yield = 59%). Mp 220−221 °C (dec.). IR (cm^{-1}): ν = 3044 (w) (CH sp^2), 2875 (w) (CH sp^3), 1626 (m) (C═N). ^{1}H NMR (400 MHz, $CDCl_3$, 298 K): δ(ppm) = 8.81 (s, br, 2H, CH═N), 8.05 (s, br, 2H, ArH), 7.66 (t, J = 7.6 Hz, 2H, ArH), 7.49−7.35 (m, 6H, ArH), 7.20−7.10 (m, 10H, ArH), 7.03−6.63 (m, 14H, ArH), 6.20 (s, br, 4H, ArH), 4.62 (s, br, 4H, CH_2). ^{1}H NMR (400 MHz, DMSO-d_6, 298 K): δ(ppm) = 8.75 (s, br, 2H, CH═N), 8.01 (d, J = 7.6 Hz, 2H, ArH), 7.84 (t, J = 7.6 Hz, 2H, ArH), 7.68 (t, J = 7.5 Hz, 2H, ArH), 7.48 (tt, J = 7.4, 1.2 Hz, 4H, ArH), 7.23 (m, 10H, ArH), 6.96 (t, J = 7.6 Hz, 4H, ArH), 6.87 (d, J = 7.6 Hz, 2H, ArH), 6.63 (s, br, 8H, ArH), 6.15 (s, br, 4H, ArH), 4.38 (s, br, 4H, CH_2). ^{13}C NMR (101 MHz, $CDCl_3$, 298 K): δ(ppm) = 168.56, 137.29, 136.50 (br), 136.26, 134.20 (br), 133.92, 131.74, 131.35 (br), 130.92, 130.29, 128.96, 128.59, 127.74, 127.30, 68.24. ^{13}C NMR (126 MHz, DMSO-d_6, 298 K): δ(ppm) = 170.77, 137.48, 136.39, 133.64, 133.15 (br), 132.58, 131.21, 130.47, 129.04, 129.01, 128.97, 128.44, 127.60, 126.95, 67.69. ^{31}P NMR (162 MHz, $CDCl_3$, 298 K): δ(ppm) = −8.62 (s, br). ^{31}P NMR (162 MHz, DMSO-d_6, 298 K): δ(ppm) = −9.14 (s, br). MS-ESI (positive ions; MeCN): m/z (%): 442 (100) $[CuL^1]^+$, 822 (60) $[CuL_2^1]^+$. Elem. anal. calcd (%) for $C_{52}H_{44}CuIN_2P_2$: C 65.79%, H 4.67%, N 2.95%; found: C 65.28%, H 4.93%, N 2.92%.

3.1.3.2. Cu(L^2)$_2$I·2H$_2$O ***(5).*** After addition of 4-methylbenzylamine (43.8 μL, 0.344 mmol), temperature was raised to 60 °C. After stirring for 5 h at 60 °C, the reaction mixture was dried and the solid recrystallized in $CHCl_3$/*n*-hexane. The resulting suspension was left at RT overnight, then it was filtrated and washed with *n*-hexane. The obtained orange solid was triturated with Et_2O and dried *in vacuo* (light orange solid, 56 mg, yield = 32%). Mp 210−213 °C (dec.). IR (cm^{-1}): ν = 3049 (w) (CH sp^2), 2834 (w) (CH sp^3), 1626 (m) (C═N). ^{1}H NMR (400 MHz, $CDCl_3$, 298 K): δ(ppm) = 8.69 (s, br, 2H, CH═N), 7.98 (s, br, 2H, ArH), 7.70−7.60 (m, 2H, ArH), 7.46−7.36 (m, 6H, ArH), 7.18 (t, J = 7.6 Hz, 8H, ArH), 7.01−6.59 (m, 14H, ArH), 6.14 (s, br, 4H, ArH), 4.63 (s, br, 4H, CH_2), 2.28 (s, 6H, CH_3). ^{1}H NMR (400 MHz, DMSO-d_6, 298 K): δ(ppm) = 8.70 (s, 2H, CH═N), 7.99 (m, 2H, ArH), 7.85 (m, 2H, ArH), 7.70 (m, 2H, ArH), 7.53−7.45 (m, 4H, ArH), 7.23 (s, br, 8H, ArH), 6.98−6.44 (m, br, 14H, ArH), 5.98 (d, J = 7.7 Hz, 4H, ArH), 4.32 (s, br, 4H, CH_2), 2.26 (s, 6H, CH_3). ^{13}C NMR (101 MHz, DMSO-d_6, 298 K): δ(ppm) = 170.22, 136.84, 135.45, 133.67, 133.34, 132.49, 131.10, 130.43, 128.95, 127.03, 64.91, 20.74. ^{31}P NMR (162 MHz, DMSO-d_6, 298 K): δ(ppm)= −9.14 (s, br). MS-ESI (positive ions; MeCN): m/z (%): 456 (100) $[CuL^2]^+$, 850 (70) $[CuL_2^2]^+$. Elem. anal. calcd (%) for $C_{54}H_{52}CuIN_2O_2P_2$: C 64.00%, H 5.17%, N 2.76%; found: C 64.01%, H 4.97%, N 2.69%. Yellow crystals of **5a** suitable for XRD analysis were obtained by slow evaporation of mother liquors.

3.1.3.3. Cu(L^3)$_2$I·4H$_2$O ***(6).*** For the synthesis, the following molar ratios were used: 3:1:3 aldehyde:CuI:amine. A solution of CuI (32.8 mg, 0.172 mmol, 1.0 equiv) in MeCN (10 mL) was added to a solution of PCHO (150 mg, 0.516 mmol, 3.0 equiv) in $CHCl_3$ (10 mL), and the resulting mixture was stirred at 50 °C for 1 h (after few minutes a yellow precipitate formed). 4-Fluorobenzylamine (59 μL, 0.516 mmol, 3.0 equiv) in MeCN (10 mL) was added and the resulting suspension was stirred at 65 °C for 5 h: the initial yellow suspension became a bright orange-red solution. The solution was allowed to cool to RT, then it was dried and recrystallized in $CHCl_3$/*n*-hexane. A yellow precipitate formed and the suspension was left at RT for 2 h, then it was filtrated, washed with *n*-hexane and dried *in vacuo*. The product was isolated as a yellow solid (101 mg, yield = 55%). Mp 229−232 °C (dec.). IR (cm^{-1}): ν = 3049 (w) (CH sp^2), 2922 (w) (CH sp^3), 1627, 1602 (m) (C═N). ^{1}H NMR (500 MHz,$CDCl_3$, 298 K): δ(ppm) = 8.85 (s, br, 2H, CH═N), 8.03 (s, br, 2H, ArH), 7.63 (t, J = 7.2 Hz, 2H, ArH), 7.41 (t, J = 7.4 Hz, 6H, ArH), 7.21 (t, J = 7.7 Hz, 8H, ArH), 7.02−6.54 (m, 14H, ArH), 6.24 (s, br, 4H, ArH), 4.63 (s, br, 4H, CH_2). ^{1}H NMR (400 MHz, DMSO-d_6, 298 K): δ(ppm) = 8.76 (s, 2H, CH═N), 7.99 (d, J = 7.6 Hz, 2H, ArH), 7.83 (t, J = 7.6 Hz, 2H, ArH), 7.68 (t, J = 7.5 Hz, 2H, ArH), 7.55−7.47 (m, 4H, ArH), 7.26 (t, J = 7.6 Hz, 8H, ArH), 6.88 (d, J = 7.6 Hz, 2H, ArH), 6.83−6.51 (m, br, 12H, ArH), 6.23 (s, br, 4H, ArH), 4.39 (s, br, 4H, CH_2). ^{13}C NMR (101 MHz, DMSO-d_6, 298 K): δ(ppm) = 162.72, 160.30, 133.55, 133.20 (br), 132.59, 131.09, 130.55, 129.20, 129.11, 128.93, 115.25, 115.03, 79.17. ^{31}P NMR (202 MHz, DMSO-d_6, 298 K): δ(ppm) = −9.11. MS-ESI (positive ions; MeCN): m/z (%): 460 (100) $[CuL^3]^+$, 858 (50) $[CuL_2^3]^+$. Elem. anal. calcd (%) for $C_{52}H_{50}CuF_2IN_2O_4P_2$: C 59.07%, H 4.77%, N 2.65%; found: C 59.07%, H 4.23%, N 2.53%.

3.1.4. General Procedure for the Synthesis of 2:1 Iminophosphine:Copper(I) Complexes Starting from Cu(NO$_3$)$_2$·3H$_2$O. An excess of copper powder (ca. 0.2 mmol) was added to a light blue solution of $Cu(NO_3)_2 \cdot 3H_2O$ (20.8 mg, 0.086 mmol, 0.5 equiv) in MeCN (15 mL); the mixture was stirred under reflux until complete decolorization of the solution (ca. 30 min). The colorless solution was quickly hot filtered to remove unreacted copper powder, then it was degassed, put under N_2 and added to a solution of PCHO (100 mg, 0.344 mmol, 2.0 equiv) in $CHCl_3$ (10 mL). The resulting yellow solution was stirred at 50 °C under N_2 for 1 h. The desired amine (0.344 mmol, 2.0 equiv) in MeCN (10 mL) was added

Downloaded from pubs.acs.org/acsodf/article-pdf/11/44/68833/6900612/acsomega.6c08107.pdf by UNIV DEGLI STUDI DI MODENA user on 17 November 2026

https://doi.org/10.1021/acsomega.6c08107
ACS Omega 2026, 11, 68833−68845

and the mixture was stirred at 50 °C under N_2 for 5 h: the initial yellow solution turned red-orange. The solution was allowed to cool to RT, then it was reduced to a small volume (3−4 mL) and Et_2O (ca. 50 mL) was added. The resulting suspension was left at 4 °C under N_2 overnight. The precipitate was filtrated, washed with Et_2O and dried *in vacuo*.

3.1.4.1. [Cu(L^1)$_2$]NO$_3$ ***(7).*** Benzylamine (37.6 μL, 0.344 mmol) was used for the synthesis. The product was isolated as a red powder (98 mg, yield = 64%). Mp 180−182 °C (dec.). IR (cm^{-1}): ν = 3049 (w) (CH sp^2), 2892 (w) (CH sp^3), 1617 (m) (C═N), 1344 (s) (NO_2 asym. str.). ^{1}H NMR (400 MHz, $CDCl_3$, 298 K): δ(ppm) = 8.73 (s, 2H, CH═N), 8.12 (d, J = 7.5 Hz, 2H, ArH), 7.77 (t, J = 7.3 Hz, 2H, ArH), 7.45 (dt, J = 34.7, 7.5 Hz, 8H, ArH), 7.21−7.09 (m, 10H, ArH), 6.89−6.70 (m, 8H, ArH), 6.59 (s, br, 4H, ArH), 5.92 (d, J = 7.5 Hz, 4H, ArH), 4.52 (s, br, 4H, CH_2). ^{1}H NMR (400 MHz, DMSO-d_6, 298 K): δ(ppm) = 8.74 (s, 2H, CH═N), 8.06−7.98 (m, 2H, ArH), 7.86 (td, J = 7.5, 1.3 Hz, 2H, ArH), 7.69 (t, J = 7.6 Hz, 2H, ArH), 7.48 (t, J = 7.4 Hz, 4H, ArH), 7.33−7.16 (m, 10H, ArH), 6.95 (t, J = 7.6 Hz, 4H, ArH), 6.87 (dt, J = 7.8, 4.0 Hz, 2H, ArH), 6.60 (s, br, 8H, ArH), 6.13 (d, J = 7.5 Hz, 4H, ArH), 4.36 (s, 4H,CH_2). ^{1}H NMR (400 MHz, CD_3OD, 298 K): δ(ppm) = 8.63 (s, 2H, CH═N), 7.98 (dq, J = 7.8, 1.8 Hz, 2H, ArH), 7.83 (td, J = 7.6, 1.3 Hz, 2H, ArH), 7.69−7.59 (m, 2H, ArH), 7.47 (t, J = 7.5 Hz, 4H, ArH), 7.28−7.15 (m, 10H, ArH), 7.01−6.25 (m, br, 14H, ArH), 6.14 (dd, J = 8.2, 1.3 Hz, 4H, ArH), 4.45 (s, 4H, CH_2). ^{13}C NMR (101 MHz, $CDCl_3$, 298 K): δ(ppm) = 170.73, 138.16, 138.12, 138.09, 137.19, 135.79, 135.73, 135.66, 134.14 (br, ovlp) 133.99 (ovlp), 132.13, 132.11, 132.08, 131.39, 130.74, 130.62, 130.43, 129.09, 129.05, 129.00, 128.64, 127.36, 127.31, 69.11. ^{13}C NMR (101 MHz, DMSO-d_6, 298 K): δ(ppm) = 170.76, 137.51, 137.48, 137.44, 136.38, 135.45, 135.38, 135.31, 133.64, 133.17 (br), 132.58, 131.20, 130.46, 129.97, 129.85, 129.73, 129.05, 129.00, 128.95, 128.44, 127.59, 126.94, 67.69. ^{31}P NMR (162 MHz, $CDCl_3$, 298 K): δ(ppm) = −7.68 (s, br). ^{31}P NMR (162 MHz, DMSO-d_6, 298 K): δ(ppm) = −9.07 (s). MS-ESI (positive ions; MeCN): m/z (%): 442 (100) [CuL^1]$^+$, 822 (10) [CuL$_2^1$]$^+$. Elem. anal. calcd (%) for $C_{52}H_{44}CuN_3O_3P_2$: C 70.62%, H 5.01%, N 4.75%; found: C 70.85%, H 4.97%, N 4.63%. Single crystals suitable for XRD analysis were obtained by slow evaporation of mother liquors.

3.1.4.2. [Cu(L^2)$_2$]NO$_3$·H$_2$O ***(8).*** 4-Methylbenzylamine (43.8 μL, 0.344 mmol) was used for the synthesis. The product was isolated as an orange sticky solid (110 mg, yield = 69%). Mp 134−137 °C (dec.). IR (cm^{-1}): ν = 3500−3300 (w) (OH), 3051 (w) (CH sp^2), 2917 (w) (CH sp^3), 1621 (m) (C═N), 1335 (s) (NO_2 asym. str.). ^{1}H NMR (500 MHz, $CDCl_3$, 298 K): δ(ppm) = 8.69 (s, 2H, CH═N), 8.09 (d, J = 6.6 Hz, 2H, ArH), 7.76 (td, J = 7.6, 1.0 Hz, 2H, ArH), 7.50 (t, J = 7.6 Hz, 2H, ArH), 7.42 (s, 4H, ArH), 7.15 (d, J = 6.4 Hz, 8H, ArH), 7.02−5.92 (m, 14H, ArH), 5.79 (d, J = 7.9 Hz, 4H, ArH), 4.46 (s, 4H, CH_2), 2.28 (s, 6H, CH_3). ^{1}H NMR (400 MHz, DMSO-d_6, 298 K): δ(ppm) = 8.71 (s, 2H, CH═N), 8.04−7.97 (m, 2H, ArH), 7.85 (td, J = 7.6, 1.3 Hz, 2H, ArH), 7.70 (t, J = 7.6 Hz, 2H, ArH), 7.49 (t, J = 7.4 Hz, 4H, ArH), 7.22 (t, J = 7.6 Hz, 8H, ArH), 6.87 (dt, J = 8.0, 4.3 Hz, 2H, ArH), 6.81−6.29 (m, br, 12H, ArH), 5.98 (d, J = 7.8 Hz, 4H, ArH), 4.32 (s, 4H, CH_2), 2.26 (s, 6H, CH_3). ^{13}C NMR (126 MHz, $CDCl_3$, 298 K): δ(ppm) = 170.30, 138.01, 137.98, 137.95, 136.90, 135.80, 135.75, 135.70, 134.14, 134.03, 132.06, 132.04, 131.35, 130.66, 130.56, 130.39, 129.29, 128.88, 127.34, 68.94, 21.36. ^{13}C NMR (126 MHz, DMSO-d_6, 298 K): δ(ppm) = 170.30, 137.38, 136.86, 135.40, 133.68, 133.32, 133.12, 132.48, 131.11, 130.45, 128.96, 128.91, 128.87, 128.84, 127.01, 67.59, 20.75. ^{31}P NMR (202 MHz, $CDCl_3$, 298 K): δ(ppm) = −7.85 (s, br). ^{31}P NMR (162 MHz, DMSO-d_6, 298 K): δ(ppm) = −9.13 (s). MS-ESI (positive ions; MeCN): m/z (%): 456 (100) [CuL^2]$^+$, 850 (30) [CuL$_2^2$]$^+$. Elem. anal. calcd (%) for $C_{54}H_{50}CuN_3O_4P_2$: C 69.70%, H 5.42%, N 4.52%; found: C 70.24%, H 5.31%, N 4.63%.

3.1.4.3. [Cu(L^3)$_2$]NO$_3$·2H$_2$O ***(9).*** 4-Fluorobenzylamine (39.3 μL, 0.344 mmol) was used for the synthesis. The product was isolated as an orange solid (113 mg, 69%). Mp 171−175 °C (dec.). IR (cm^{-1}): ν = 3057 (w) (CH sp^2), 2979 (w) and 2853 (w) (CH sp^3), 1621 (m), 1604 (m) (C═N), 1364, 1323 (s) (NO_2 asym. str.). ^{1}H NMR (400 MHz, $CDCl_3$, 298 K): δ(ppm) = 8.78 (s, 2H, CH═N), 8.14 (dq, J = 7.7, 1.8 Hz, 2H, ArH), 7.76 (td, J = 7.5, 1.3 Hz, 2H, ArH), 7.47 (dt, J = 18.3, 7.5 Hz, 6H, ArH), 7.19 (t, J = 7.6 Hz, 8H, ArH), 6.91−6.18 (m, br, 14H, ArH), 5.90−5.78 (m, 4H, ArH), 4.50 (s, br, 4H, CH_2).^{1}H NMR (400 MHz, DMSO-d_6, 298 K): δ(ppm) = 8.76 (s, 2H, CH═N), 8.05−7.98 (m, 2H, ArH), 7.85 (td, J = 7.5, 1.2 Hz, 2H, ArH), 7.74−7.66 (m, 2H, ArH), 7.51 (t, J = 7.5 Hz, 4H, ArH), 7.26 (t, J = 7.6 Hz, 8H, ArH), 6.88 (dt, J = 7.9, 4.1 Hz, 2H, ArH), 6.79−6.55 (m, br, 12H, ArH), 6.17 (dd, J = 8.4, 5.4 Hz, 4H, ArH), 4.36 (s, 4H, CH_2). ^{13}C NMR (101 MHz, $CDCl_3$, 298 K): δ(ppm) = 171.01, 163.32, 160.88, 138.31, 138.27, 138.23, 135.76, 135.69, 135.62, 134.05 (br), 133.88, 133.31, 133.28, 132.14, 132.12, 132.09, 131.46, 130.63, 130.56, 130.44, 130.31, 129.05, 129.01, 128.97, 115.52, 115.30, 68.33. ^{13}C NMR (101 MHz, DMSO-d_6, 298 K): δ(ppm) = 171.01, 162.77, 160.34, 137.53, 137.50, 137.46, 135.42, 135.35, 135.28, 133.62, 133.15 (br), 132.73, 132.58, 132.55, 131.20, 130.60, 129.72, 129.60, 129.48, 129.10, 129.02, 129.00, 128.95, 128.90, 115.28, 115.07, 66.98. ^{31}P NMR (162 MHz, $CDCl_3$, 298 K): δ(ppm) = −7.54 (s, br). ^{31}P NMR (162 MHz, DMSO-d_6, 298 K): δ(ppm) = −8.96 (s). MS-ESI (positive ions; MeCN): m/z (%): 460 (100) [CuL^3]$^+$, 858 (60) [CuL$_2^3$]$^+$. Elem. anal. calcd (%) for $C_{52}H_{46}CuF_2N_3O_5P_2$: C 65.30%, H 4.85%, N 4.39%; found: C 65.54%, H 4.86%, N 4.20%.

3.1.5. Synthesis of PCHO:Copper(I) Complexes.

3.1.5.1. [Cu(μ-I)(MeCN)L^a]$_2$. The reaction was performed under N_2 atmosphere and the solvents were degassed prior to use. To a solution of PCHO (L^a, 100 mg, 0.344 mmol, 1.0 equiv) in $CHCl_3$ (10 mL) was added a solution of CuI (65.9 mg, 0.346 mmol, 1.0 equiv) in MeCN (10 mL) and the resulting mixture was stirred at 50 °C for 1 h. The obtained yellow suspension was allowed to cool to RT, then it was reduced to half volume. The suspension was left at 4 °C under N_2 for 1 h, then it was filtrated, washed with cold MeCN and dried *in vacuo*. The product was isolated as a yellow powder (132 mg, yield = 74%). Mp 210−212 °C. IR (cm^{-1}): ν = 2921 (w), 2829(w), 2747 (w) (CH), 2295 (w), 2270 (w) (C≡N), 1688 (s) (C═O). ^{1}H NMR (400 MHz, $CDCl_3$, 298 K): δ(ppm) = 10.09 (s, br, 2H, CH═O), 7.94 (d, J = 7.4 Hz, 2H, ArH), 7.62−7.27 (m, 24H, ArH), 7.00 (d, J = 7.6 Hz, 2H, ArH), 2.01 (s, 6H, $\underline{CH_3}$-CN). ^{31}P NMR (162 MHz, $CDCl_3$, 298 K): δ(ppm) = −0.13 (s, br). MS-ESI (positive ions; MeCN): m/z (%): 353 (100) [Cu(L^a)]$^+$, 643 (40) [Cu(L^a)$_2$]$^+$. Elem. anal. calcd (%) for $C_{42}H_{36}Cu_2I_2N_2O_2P_2$: C 48.34%, H 3.48%, N 2.68%; found: C 47.88%, H 3.38%, N 2.16%.

3.1.5.2. Cu(L^a)$_2$I. The reaction was performed under N_2 atmosphere and the solvents were degassed prior to use. To a solution of PCHO (100 mg, 0.344 mmol, 2.0 equiv) in $CHCl_3$ (10 mL) was added a solution of CuI (32.8 mg, 0.172 mmol, 1.0 equiv) in MeCN (10 mL) and the resulting mixture was stirred at 50 °C for 1 h. The obtained yellow suspension was allowed to cool to RT, then it was reduced to half volume. The suspension was left at 4 °C under N_2 for 2 h, then it was filtrated, washed with cold MeCN and dried *in vacuo*. The product was isolated as a yellow powder (100 mg, yield = 75%). Mp 254−256 °C. IR (cm^{-1}): ν = 3061 (w), 2921 (w) (CH sp^2), 2838 (w), 2744 (w) (aldehyde CH), 1696 (m), 1674 (s) (C═O). ^{1}H NMR (400 MHz, $CDCl_3$, 298 K): δ(ppm) = 9.98 (s, br, 2H, CH═O), 7.89 (d, J = 7.7 Hz, 2H, ArH), 7.60 (td, J = 7.5, 1.2 Hz, 2H, ArH), 7.55−7.33 (m, 16H, ArH), 7.28 (s, 4H, ArH), 7.24 (s, 2H, ArH), 7.01 (d, J = 7.6 Hz, 2H, ArH). ^{31}P NMR (162 MHz, $CDCl_3$, 298 K): δ(ppm) = −1.53 (s, br). MS-ESI (positive ions; MeCN): m/z (%): 290 (70) [L^a]$^+$, 353 (85) [Cu(L^a)]$^+$, 643 (100) [Cu(L^a)$_2$]$^+$. Elem. anal. calcd (%) for $C_{38}H_{30}CuIO_2P_2$: C 59.19%, H 3.92%; found: C 59.62%, H 3.98%. Single crystals suitable for XRD analysis were obtained by slow evaporation of a solution of the complex in $CHCl_3$.

3.1.5.3. [Cu(L^a)$_2$NO$_3$]. To a light blue solution of $Cu(NO_3)_2·3H_2O$ (20.8 mg, 0.086 mmol, 0.5 equiv) in MeCN (15 mL) was added an excess of copper powder (ca. 0.2 mmol) and the mixture was stirred under reflux until complete decolorization of the solution (ca. 30 min). The colorless solution was quick hot filtered to remove unreacted copper powder, then it was degassed, put under N_2 and added to a solution of PCHO (100 mg, 0.344 mmol, 2.0 equiv) in $CHCl_3$ (10 mL). The resulting yellow solution was stirred at 50 °C

Downloaded from pubs.acs.org/acsodf/article-pdf/11/44/68833/6900612/acsomega.6c08107.pdf by UNIV DEGLI STUDI DI MODENA user on 17 November 2026

https://doi.org/10.1021/acsomega.6c08107
ACS Omega 2026, 11, 68833−68845

under N_2 for 1 h. The solution was allowed to cool to RT, then it was reduced to a small volume (3−4 mL) and Et_2O (ca. 50 mL) was added. The mixture was left at −20 °C under N_2 overnight. The precipitate was filtrated, washed with Et_2O and dried *in vacuo*. The product was isolated as a yellow crystalline solid (92 mg, yield = 76%). Mp 193−195 °C (dec.). IR (cm^{-1}): ν = 3061 (w) (CH sp^2), 2852 (w), 2757 (w) (CH aldehyde), 1692 (m), 1670 (s) (C═O), 1434 (s) (NO stretch), 1286 (s) (NO_2 asym. stretch). ^1H NMR (400 MHz, DMSO-d_6, 298 K): δ(ppm) = 9.97 (s, br, 2H, CH═O), 8.00 (s, br, 2H, ArH), 7.73 (dtd, J = 18.2, 7.4, 1.5 Hz, 4H, ArH), 7.56−6.96 (m, 20H, ArH), 6.85 (d, J = 7.5 Hz, 2H, ArH). MS-ESI (positive ions; MeCN): m/z (%): 353 (100) $[Cu(L^a)]^+$, 643 (65) $[Cu(L^a)_2]^+$. Elem. anal. calcd (%) for $C_{38}H_{30}CuNO_5P_2$: C 64.63%, H 4.28%, N 1.98%; found: C 65.00%, H 4.35%, N 2.07%. Single crystals for X-ray diffraction analysis were selected from the sample.

3.2. Crystallography

Single crystal X-ray diffraction analysis were performed on selected single crystals on a Bruker D8 Venture diffractometer equipped with a kappa goniometer and a Photon II detector. Low-temperature data collections were performed under nitrogen flux employing an Oxford cryostream. Microfocused Mo−Kα radiation (λ=0.71073 Å) was used for (**3**) and $[\mathbf{Cu(L^a)_2NO_3}]$, and Cu Kα radiation (λ = 1.54178 Å) for (**2**), (**5a**), and (**7**) for data acquisition. Lorentz polarization and absorption correction were applied. Data were reprocessed using APEX v3 software. Structures were solved by direct methods using SHELXT[29] and refined by full-matrix least-squares on all F^2 using SHELXL[30] implemented in Olex2.15.[31] Anisotropic displacement parameters were refined except for hydrogen atoms, which were introduced in calculated positions riding on their carrier atoms. The data deposited with the Cambridge Structural Database have the deposition numbers CCDC 2560043−2560047. The data can be obtained free of charge via www.ccdc.cam.ac.uk/data_request/cif or by emailing data_request@ccdc.cam.ac.uk, or by contacting The Cambridge Crystallographic Data center, 12 Union Road, Cambridge CB2 1EZ, UK. (http://www.ccdc.cam.ac.uk/data_request/cif).

3.3. Biological Studies

3.3.1. Microbial Strains and Growth Conditions. Reference strains of *S. aureus* (ATCC 25923), *E. coli* (ATCC 25922) and *C. albicans* (ATCC 10231) were used in the study as microbial models. The strains were obtained from the American Type Culture Collection (ATCC, Manassas, VA, USA). Bacterial cultures were grown on 5% blood agar plates (Biolife Italiana S.r.l., Milan, Italy) at 37 °C while fungal cultures on Sabouraud Dextrose Agar (Biolife Italiana S.r.l., Milan, Italy) at 37 °C.

3.3.2. Metal Complexes and Reference Drugs. The dry powder of the iminophosphine copper(I) complexes was dissolved in 100% DMSO at 20 mM and then diluted with the appropriate cell culture medium to achieve the required concentrations. Ciprofloxacin, fluconazole, and cisplatin, purchased from Sigma-Aldrich (St. Louis, MO, USA), were used as reference drugs in the biological assays (Table S51).

3.3.3. Determination of the MIC and IC_{50} Values. The antimicrobial activity of the compounds was evaluated *in vitro* by determining the Minimum Inhibitory Concentration (MIC) using a well-established broth microdilution method in compliance with the Clinical and Laboratory Standards Institute (CLSI) guidelines. Briefly, microbial inocula were adjusted to 0.5 McFarland (10^8 CFU/mL) in phosphate-buffered saline (PBS); bacterial suspensions were subsequently diluted 1:200 in Mueller−Hinton broth (MH CondaLab, Laboratorios Conda S.A., Madrid, Spain), whereas fungal suspensions were diluted 1:20 in RPMI-1640 medium (Gibco, ThermoFisher Scientific Inc., Waltham, MA, USA), containing 1.8% glucose, 0.3% levo-glutamine buffered to pH 7.0 with MOPS at 0.165 M. Aliquots of 100 μL of the microbial suspensions were added to 96-well microplates containing 100 μL of the test compounds, 2-fold serially diluted to final concentrations ranging from 100 to 0.78 μM. Positive controls (microbial suspensions in growth medium), negative controls (medium only), and solvent controls were included in all experiments. Ciprofloxacin and fluconazole were used as reference antimicrobial agents. The plates were incubated at 37 °C for 24 h, and subsequently the optical density was measured at 630 nm.

MIC values were defined as the minimum concentrations required to inhibit 90% of microbial growth relative to the positive controls. For the most active compounds, IC_{50} values were also determined These values, corresponding to the concentration that reduce microbial growth by 50%, were calculated by nonlinear regression analysis. Specifically, dose−response curves were generated by plotting the percentage of growth inhibition, normalized to the positive control (100% growth) against the logarithm of the tested compounds concentrations. All statistical analyses and curve fittings were performed using GraphPad Prism software, version 9.4.1.[32]

3.3.4. Cell Viability Assay. Vero (ATCC CCL-81) and Caco-2 (ATCC HTB-37) cell lines were used as experimental models to investigate the effects of the different metal complexes on non-malignant mammalian cells and malignant human cells, respectively. Briefly, cells were cultured at 37 °C with 5% CO_2 in Eagle's Minimum Essential medium (EMEM, Lonza, Walkersville, MD, USA) supplemented with 10% fetal bovine serum (FBS; Microgen Laboratory Research srl), 100 μg/mL penicillin, and 100 μg/mL streptomycin. For the experiments, cells were seeded into 96-well plates at 10^4 cells/well, and incubated at 37 °C for 24 h. The culture medium was then removed, and cell monolayers were incubated with 100 μL of fresh medium containing 2-fold serial dilutions of the compounds at the final concentrations ranging from 100 to 0.78 μM. Untreated cells were used as positive controls, whereas cells treated with 1% Triton X-100 served as negative controls. Cisplatin was included as reference compound.

Cell viability was determined using a well-established Neutral red uptake assay.[33] After 48 h of treatment, the culture medium was removed, the cell monolayers were washed with PBS, and 100 μL of fresh medium containing 1:100 dilution of Neutral Red solution (4 mg/mL) was added. Following 3 h of incubation at 37 °C, the medium was discarded and cells were washed twice with PBS before adding 100 μL of destaining solution (50% ethanol, 49% water, and 1% glacial acetic acid) to each well. The plates were incubated under constant agitation (300 rpm) for 20−45 min, followed by the measurement of absorbance at 550 nm. Data were expressed as the percentage of cell viability relative to the untreated controls. The CC_{50} values were obtained from the corresponding dose−response curves, as previously reported for IC_{50} determination.

3.3.5. Hemolytic Activity Assay. The hemolytic potential of the iminophosphine copper(I) complexes was determined by quantifying the hemoglobin released upon the lysis of human red blood cells (hRBCs). Fresh hRBCs, obtained from anonymous donor, were isolated via centrifugation, washed with PBS, and adjusted to a final concentration of 4% (w/v) in the same buffer. For the assay, 100 μL of hRBCs suspension was mixed with an equal volume of the test compounds in a 96−well microplate, using 2-fold serial dilutions ranging from 100 to 0.78 μM. Since the solubilized samples exhibited intrinsic color, background controls consisting of the corresponding compound concentrations without hRBCs were included to assess potential interference with absorption measurements. Following the incubation at 37 °C for 1 h, the supernatants were transferring in a new 96-well plate and the released hemoglobin was the quantified at 405 nm. Untreated hRBCs in PBS were used as negative control (0% hemolysis), whereas hRBCs treated with 1% Triton X-100 served as the positive control (100% hemolysis). The percentage of hemolysis was calculated $[OD_{405nm}\ (\text{sample}) - OD_{405nm}\ (\text{background})]/[OD_{405nm}\ (\text{positive control}) - OD_{405nm}\ (\text{negative control})] \times 100$. Finally, the Minimal Hemolytic Concentration (MHC) was defined as the lowest concentration of compound inducing 10% hemolysis.

3.3.6. Plasmid DNA Interaction Assay. The interaction between the iminophosphine copper(I) complexes and a plasmid DNA was investigated via agarose gel electrophoresis. Briefly, 200 ng of pmaxGFP plasmid (3527 bp; Lonza, Basel, Switzerland) were incubated with the test compounds (100 μM) in a Tris-HCl buffer (5 mM Tris-HCl, 50 mM NaCl, pH 7.20). Cisplatin (100 μM) was used as DNA-damage control, while the plasmid in the Tris-HCl buffer as negative control. After a 2 h incubation at 37 °C, all the reactions

Downloaded from pubs.acs.org/acsodf/article-pdf/11/44/68833/6900612/acsomega.6c08107.pdf by UNIV DEGLI STUDI DI MODENA user on 17 November 2026

https://doi.org/10.1021/acsomega.6c08107
ACS Omega 2026, 11, 68833−68845

were stopped by adding 5 μL of loading buffer solution. The samples were subsequently analyzed using 1% agarose gel electrophoresis to assess any DNA modifications or binding events.

4. CONCLUSIONS

Despite the limited number of compounds investigated, some general considerations can be drawn about their biological activity. In $[\mathbf{CuL_2^a(NO_3)}]$, the ligand L^a is simply PCHO, that behaves as P-monodentate, and the aldehyde oxygen, with low affinity for the soft copper(I) ion, does not coordinate. It is interesting to note that $[\mathbf{CuL_2^a(NO_3)}]$ did not exhibit any detectable biological activity, including hemolytic effects on hRBCs, suggesting a lack of interaction with biological membranes as well as with plasmid DNA.

The other complexes (**4**)−(**9**) showed antibacterial activity against *S. aureus*; however, this effect was observed at concentrations that were also cytotoxic toward Vero cells, indicating poor selectivity and therefore limited potential as selective antibacterial agents.

Regarding their potential antiproliferative activity, the data obtained in the cellular assays indicate that iodide-containing complexes (**4**)−(**6**) display lower CC_{50} values in Caco-2 cells compared to Vero cells, suggesting a preferential cytotoxic effect toward malignant cells. In contrast, nitrate-containing complexes (**7**)−(**9**) exhibited the opposite trend. Taken together with the hemolysis results, which indicate limited membrane disruption at bioactive concentrations, these findings point to a possible intracellular mechanism of action such as their interaction with DNA molecules. Although at a qualitative level and under cell-free conditions, some complexes (**4**)−(**6**) induced changes in plasmid DNA topology consistent with a DNA strand-scission activity and in agreement with the antiproliferative property observed in Caco-2 cells. However, the mechanism underlying this effect cannot be established from the present experimental data. Further studies, including more detailed mechanistic investigations, are therefore required to elucidate the molecular pathways responsible for the observed DNA damage and to clarify its possible contribution to the antiproliferative activity of these complexes.

■ ASSOCIATED CONTENT

Data Availability Statement

Data supporting the findings of this study are available within the article and its Supporting Information.

Supporting Information

The Supporting Information is available free of charge at https://pubs.acs.org/doi/10.1021/acsomega.6c08107.

Figure S1; (a) Comparison between the FT-IR spectra of $[\mathbf{Cu(\mu\text{-}I)L^1}]_2$ (blue) and **PCHO** (red); (b) comparison of the FT-IR spectrum of complex $[\mathbf{Cu(\mu\text{-}I)L^1}]_2$ (red) with ligand $\mathbf{L^1}$ (blue); Figure S2: FT-IR spectrum of (**2**); Figure S3: FT-IR spectrum of (**3**); Figure S4: X-ray crystallographic data for compound (**2**); Figure S5: ORTEP diagram of the crystal structure of complex (**3**); Figure S6: (a) ^{1}H NMR (400 MHz, 298 K); (b) ^{31}P NMR (162 MHz, 298 K) spectra of $\mathbf{L^1}$ (top) and of the complex (**1**) (bottom) in $CDCl_3$; (c) ^{31}P NMR (162 MHz, 298 K) spectrum of (**1**) immediately after preparation of the sample (top) and after 1 day (bottom) in DMSO-d_6; Figure S7: ^{1}H NMR (400 MHz, 298 K) and ^{31}P NMR (162 MHz, 298 K) spectra of (**2**) in $CDCl_3$; Figure S8: ^{1}H NMR (400 MHz, $CDCl_3$, 298 K) spectrum of (**3**); Figure S9: ^{31}P NMR (162 MHz, chloroform-*d*, 298 K) spectrum of (**3**); Figure S10: ESI-MS spectrum (positive ions) for complex (**1**) in acetonitrile; Figure S11: ESI-MS spectrum (positive ions) for (**2**) in acetonitrile; Figure S12: ESI-MS spectrum (positive ions) for (**3**) in acetonitrile; Figure S13. (a) Synthesis of the complex $[\mathbf{Cu(\mu\text{-}I)(MeCN)L^a}]_2$, $\mathbf{L^a}$ = PCHO; Figure S14: ^{1}H NMR (400 MHz, $CDCl_3$, 298 K) spectrum of $[\mathbf{Cu(\mu\text{-}I)(MeCN)L^a}]_2$; Figure S15: ^{31}P NMR (162 MHz, $CDCl_3$, 298 K) spectrum of $[\mathbf{Cu(\mu\text{-}I)(MeCN)L^a}]_2$; Figure S16: ESI-MS spectrum (positive ions) for $[\mathbf{Cu(\mu\text{-}I)(MeCN)L^a}]_2$ in acetonitrile; Figure S17: (a) calculated (in red) and experimental (in black) powder diffractogram of complex $[\mathbf{Cu(\mu\text{-}I)(MeCN)L^a}]_2$; (b) ORTEP diagram of the crystal structure of $[\mathbf{Cu(\mu\text{-}I)(MeCN)L^a}]_2$; Figure S18: FT-IR spectrum of (**4**); Figure S19: FT-IR spectrum of (**5**); Figure S20: FT-IR spectrum of (**6**); Figure S21: (a) ^{1}H NMR (400 MHz, 298 K) and (b) ^{31}P NMR (162 MHz, 298 K) spectra of $\mathbf{L^1}$ (top), complex (**1**) (middle), and complex (**4**) (bottom) in $CDCl_3$; Figure S22: (top) ^{1}H NMR (400 MHz, $CDCl_3$, 298 K) spectrum of (**4**) immediately after preparation of the sample (purple), after 1 day (blue-green), after 2 days (green) and after 1 week (red). (bottom) ^{31}P NMR (162 MHz, $CDCl_3$, 298 K) spectrum of complex (**4**) immediately after preparation of the sample (purple), after 1 day (blue-green), after 2 days (green) and after 1 week (red); Figure S23: ^{1}H NMR (400 MHz, DMSO-d_6, 298 K) spectrum of (**4**); Figure S24: ^{1}H NMR (400 MHz, DMSO-d_6, 298 K) spectrum of (**4**) immediately after preparation of the sample (top), after 1 day (middle) and after 2 days (bottom); Figure S25: ^{1}H NMR (400 MHz, DMSO-d_6, 298 K) spectrum of (**5**); Figure S26: ^{31}P NMR (162 MHz, DMSO-d_6, 298 K) spectrum of (**5**); Figure S27: ^{1}H NMR (400 MHz, DMSO-d_6, 298 K) spectrum of (**6**); Figure S28: ^{31}P NMR (202 MHz, DMSO-d_6, 298 K) spectrum of (**6**); Figure S29: ESI-MS spectrum (positive ions) for (**4**) in acetonitrile; Figure S30: ESI-MS spectrum (positive ions) for (**5**) in acetonitrile; Figure S31: ESI-MS spectrum (positive ions) for (**6**) in acetonitrile; Figure S32: X-ray crystallographic data and ORTEP representation for compound (**5a**); Figure S33: FT-IR spectrum of $[\mathbf{Cu(L^a)_2I}]$; Figure S34: (top) ^{1}H NMR (400 MHz, 298 K) and (bottom) ^{31}P NMR (162 MHz, 298 K) spectra of $[\mathbf{Cu(L^a)_2I}]$ in $CDCl_3$; Figure S35: ESI-MS spectrum (positive ions) for $[\mathbf{Cu(L^a)_2I}]$ in acetonitrile; Figure S36: (top) FT-IR spectra of the complex (**7**) (in red) and $\mathbf{L^1}$ (in blue); (bottom) FT-IR spectrum of (**7**); Figure S37: FT-IR spectrum of (**8**); Figure S38: FT-IR spectrum of (**9**); Figure S39: (top) ^{1}H NMR (400 MHz, $CDCl_3$, 298 K) and (bottom) ^{31}P NMR (162 MHz, $CDCl_3$, 298 K) spectra of (**7**); Figure S40: (a) ^{1}H NMR (400 MHz, 298 K) spectrum of (**7**) recorded in DMSO-d_6; (b) ^{31}P NMR (162 MHz, 298 K) spectrum of (**7**) in DMSO-d_6 measured immediately after preparation of the sample (purple), after 24 h (blue-green), 48 h (green) and 1 week (red); Figure S41: ^{1}H NMR (400 MHz, DMSO-d_6, 298 K) spectrum of (**8**); Figure S42: ^{31}P NMR (162 MHz, DMSO-d_6, 298 K) spectrum of (**8**); Figure S43: ^{1}H NMR (400 MHz, DMSO-d_6, 298

Downloaded from pubs.acs.org/acsodf/article-pdf/11/44/68833/6900612/acsomega.6c08107.pdf by UNIV DEGLI STUDI DI MODENA user on 17 November 2026

https://doi.org/10.1021/acsomega.6c08107
ACS Omega 2026, 11, 68833−68845

K) spectrum of (**9**); Figure S44: ^{31}P NMR (162 MHz, DMSO-d_6, 298 K) spectrum of (**9**); Figure S45: ESI-MS spectra (positive ions) for (**7**) (top), (**8**) and (**9**) (bottom) in acetonitrile; Figure S46: X-ray crystallographic data and ORTEP for compound (**7**); Figure S47: FT-IR spectra of $[Cu(L^a)_2NO_3]$ (in blue) and PCHO (in red); Figure S48: X-ray crystallographic data and ORTEP diagram for compound $[Cu(L^a)_2NO_3]$; Figure S49: ^{1}H NMR (400 MHz, DMSO-d_6, 298 K) spectrum of $[Cu(L^a)_2NO_3]$; Figure S50: ESI-MS spectrum (positive ions) for $[Cu(L^a)_2NO_3]$ in acetonitrile; Table S51: IC_{50} and CC_{50} values (mean ± standard deviation) of the reference drug controls; Table S52: IC_{50} values (in μM) of copper(I) iminophosphine complexes; Table S53: CC_{50} values (in μM) of copper(I) iminophosphine complexes; Figure S54: Dose−response curves of the complexes obtained in Caco-2 cells; Table S55: CC_{50} values determined in Caco-2 cells and hemolytic activity (%) measured at the corresponding CC_{50} concentrations (PDF)

Accession Codes

The data deposited with the Cambridge Structural Database have the deposition numbers CCDC 2560043−2560047. They can be obtained free of charge via www.ccdc.cam.ac.uk/data_request/cif or by emailing data_request@ccdc.cam.ac.uk, or by contacting The Cambridge Crystallographic Data center, 12 Union Road, Cambridge CB2 1EZ, UK. (http://www.ccdc.cam.ac.uk/data_request/cif)

AUTHOR INFORMATION

Corresponding Author

Mauro Carcelli − *Department of Chemistry, Life Sciences, Environmental Sustainability, University of Parma, 43124 Parma, Italy;* orcid.org/0000-0001-5888-4556; Email: mauro.carcelli@unipr.it

Authors

Alessio Zavaroni − *Department of Chemistry, Life Sciences, Environmental Sustainability, University of Parma, 43124 Parma, Italy;* orcid.org/0000-0002-9761-7247

Luca Rigamonti − *Dipartimento di Scienze Chimiche e Geologiche, Università di Modena e Reggio Emilia, 41125 Modena, Italy;* orcid.org/0000-0002-9875-9765

Giorgio Pelosi − *Department of Chemistry, Life Sciences, Environmental Sustainability, University of Parma, 43124 Parma, Italy;* orcid.org/0000-0002-7946-0602

Lorenzo Verderi − *Department of Chemistry, Life Sciences, Environmental Sustainability, University of Parma, 43124 Parma, Italy;* orcid.org/0009-0001-1316-4579

Matteo Incerti − *Food and Drug Department, University of Parma, 43124 Parma, Italy*

Lisa Menegaldo − *Department of Pharmacy and Biotechnology, University of Bologna, 40138 Bologna, Italy*

Diego Montagner − *Department of Chemistry, Maynooth University, W23 X021 Maynooth, Ireland;* orcid.org/0000-0002-1034-9623

Dominga Rogolino − *Department of Chemistry, Life Sciences, Environmental Sustainability, University of Parma, 43124 Parma, Italy;* orcid.org/0000-0003-2295-5783

Francesca Bonvicini − *Department of Pharmacy and Biotechnology, University of Bologna, 40138 Bologna, Italy*

Complete contact information is available at: https://pubs.acs.org/10.1021/acsomega.6c08107

Author Contributions

A.Z. and L.M.: Writing—original draft, investigation, formal analysis, data curation. G.P. and L.V.: Writing—review and editing, formal analysis. D.M.: Writing—review and editing, supervision. D.R., F.B., and M.C.: Writing—original draft, supervision, investigation, funding acquisition, data curation, conceptualization.

Funding

This research was granted by University of Parma through the action "Bando di Ateneo 2023 per la ricerca".

Notes

The authors declare no competing financial interest.

ACKNOWLEDGMENTS

This work has benefited from the equipment and framework of the COMP-HUB and COMP-R Initiative, funded by the 'Departments of Excellence' program of the Italian Ministry for Education, University and Research (MIUR, 2018−2022 and MUR, 2023−2027).

REFERENCES

(1) Murray, C. J. L.; Ikuta, K. S.; Sharara, F.; Antimicrobial Resistance Collaborators; et al. Global burden of bacterial antimicrobial resistance in 2019: a systematic analysis. *Lancet* **2022**, *10325*, 629−655.

(2) Liu, Q.; Liu, L.; Yin, L.; Guo, J.; Liao, X.; Li, J.; Zhang, Z. S. Metal complexes against multidrug-resistant bacteria: recent advances (2020-present). *Dalton Trans.* **2025**, *54*, 17025−17059.

(3) Wang, C.; Wei, X.; Zhong, L.; Chan, C. L.; Li, H.; Sun, H. Metal-Based Approaches for the Fight against Antimicrobial Resistance: Mechanisms, Opportunities, and Challenges. *J. Am. Chem. Soc.* **2025**, *147*, 12361−12380.

(4) Tsvetkov, P.; Coy, S.; Petrova, B.; Dreishpoon, M.; Verma, A.; Abdusamad, M.; Rossen, J.; et al. Copper induces cell death by targeting lipoylated TCA cycle proteins. *Science* **2022**, *375* (6586), 1254−1261.

(5) Fu, Y.; Chang, F. M. J.; Giedroc, D. P. Copper Transport and Trafficking at the Host−Bacterial Pathogen Interface. *Acc. Chem. Res.* **2014**, *47* (12), 3605−3613.

(6) Wang, W.; Gui, H.; Wei, X.; Liu, H.; Wang, X. Cuproptosis to Cuproptosis-Like: Therapeutic Strategies for Bacterial Infection. *Adv. Mater.* **2025**, *37* (37), No. e2506119.

(7) Mei, J.; Xu, D.; Wang, L.; Kong, L.; Liu, Q.; Li, Q.; Zhang, X.; Su, Z.; Hu, X.; Zhu, W.; Ye, M.; Wang, J.; Zhu, C. Biofilm Microenvironment-Responsive Self-Assembly Nanoreactors for All-Stage Biofilm Associated Infection through Bacterial Cuproptosis-like Death and Macrophage Re-Rousing. *Adv. Mater.* **2023**, *35*, No. 2303432.

(8) Beaudelot, J.; Oger, S.; Perusko, S.; Phan, T. A.; Teunens, T.; Moucheron, C.; Evano, G. Photoactive Copper Complexes: Properties and Applications. *Chem. Rev.* **2022**, *122* (22), 16365−16609.

(9) Rosko, M. C.; Wheeler, J. P.; Alameh, R.; Faulkner, A. P.; Durand, N.; Castellano, F. N. Enhanced Visible Light Absorption in Heteroleptic Cuprous Phenanthrolines. *Inorg. Chem.* **2024**, *63* (3), 1692−1701.

(10) Gu, L.; Xiong, Z.; Zhong, Y.; Chen, Z. Reticular synthesis of high-connectivity metal−organic frameworks with Kuratowski-type building blocks. *J. Am. Chem. Soc.* **2026**, *148* (1), 99−105.

(11) Starosta, R. Tris(aminomethyl)phosphines and Their Copper-(I) (Pseudo)halide Complexes with Aromatic Diimines-A Critical Retrospection. *Pharmaceuticals* **2023**, *16* (5), No. 766.

Downloaded from pubs.acs.org/acsodf/article-pdf/11/44/68833/6900612/acsomega.6c08107.pdf by UNIV DEGLI STUDI DI MODENA user on 17 November 2026

(12) Caviglia, M.; Li, Z.; Santini, C.; Del Gobbo, J.; Cimarelli, C.; Du, M.; Dolmella, A.; Pellei, M. New Cu(II), Cu(I) and Ag(I) Complexes of Phenoxy-Ketimine Schiff Base Ligands: Synthesis, Structures and Antibacterial Activity. *Molecules* **2025**, *30*, No. 1893.
(13) Bernardi, T.; Badel, S.; Mayer, P.; Groelly, J.; de Fremont, P.; Jacques, B.; Braunstein, P.; Teyssot, M. L.; Gaulier, C.; Cisnetti, F.; Gautier, A.; Roland, S. High-Throughput Screening of Metal-N-Heterocyclic Carbene Complexes against Biofilm Formation by Pathogenic Bacteria. *Chem. Med. Chem.* **2014**, *9*, 1140−1144.
(14) Touj, N.; Chakchouk-Mtibaa, A.; Mansour, L.; Harrath, A. H.; Al-Tamimi, J.; Mellouli, L.; Ozdemir, I.; Yasar, S.; Hamdi, N. Synthesis, spectroscopic properties and biological activity of new Cu(I) N-Heterocyclic carbene complexes. *J. Mol. Struct.* **2019**, *1181*, 209−219.
(15) Traut-Johnstone, T.; Kanyanda, S.; Kriel, F. H.; Viljoena, T.; Kotze, P. D. R.; van Zyl, W. E.; Coates, J.; Rees, D. J. G.; Meyer, M.; Hewer, R.; Williams, D. B. G. Heteroditopic P,N ligands in gold(I) complexes: Synthesis, structure and cytotoxicity. *J. Inorg. Biochem.* **2015**, *145*, 108−120.
(16) Isai Ortega-Gaxiola, J.; Valdés, H.; Rufino-Felipe, E.; Toscano, R. A.; Morales-Morales, D. Synthesis of Pd(II) complexes with P-N-OH ligands derived from 2-(diphenylphosphine)-benzaldehyde and various aminoalcohols and their catalytic evaluation on Suzuki-Miyaura couplings in aqueous media. *Inorg. Chim. Acta* **2020**, *504*, No. 119460.
(17) Mogorosi, M. M.; Mahamo, T.; Moss, J. R.; Mapolie, S. F.; Slootweg, J. C.; Lammertsma, K.; Smith, G. S. Neutral palladium(II) complexes with P,N Schiff-base ligands: Synthesis, characterization and catalytic oligomerisation of ethylene. *J. Organomet. Chem.* **2011**, *696*, 3585−3592.
(18) Chen, L.; Huo, S.; Wang, P.; Bai, X.; Gao, Y.; Yang, Y. Synthesis and characterization of bis(imino)phosphine [NPN] ligands and their copper(I) halide complexes. *Polyhedron* **2025**, *265*, No. 117278.
(19) Huo, S.; Bai, X.; Wang, P.; Gao, Y.; Yang, Y. Synthesis and catalytic properties of copper(I) complexes with imino- and aminophosphine ligands. *Inorg. Chim. Acta* **2026**, *589*, No. 122884.
(20) Süß, J.; Monkowius, U.; Zabel, M. Diiodido-bis{*N*-[2-(diphenylphosphino)benzylidene]benzylamine-κ^2N,P}dicopper(I). *Molbank* **2024**, *2024*, No. M1808.
(21) Aguirrechu-Comerón, A.; Hernández-Molina, R.; González-Platas, J. Structure of Two New Compounds of Copper(I) Iodide with N-Donor and P-Donor Ligands. *J. Struct. Chem.* **2018**, *59*, 943−948.
(22) Kritchenkov, I. S.; Shakirova, J. R.; Tunik, S. P. Efficient one-pot green synthesis of tetrakis(acetonitrile)copper(I) complex in aqueous media. *RSC Adv.* **2019**, *9* (27), 15531−15535.
(23) Curtis, N. F.; Curtis, Y. M. Some Nitrato-Amine Nickel(II) Compounds with Monodentate and Bidentate Nitrate Ions. *Inorg. Chem.* **1965**, *4*, 804−809.
(24) Bonvicini, F.; Locatelli, A.; Morigi, R.; Leoni, A.; Gentilomi, G. A. Isatin bis-indole and bis-imidazothiazole hybrids: synthesis and antimicrobial activity. *Molecules* **2022**, *27* (18), No. 5781.
(25) Seghetti, F.; Ocello, R.; Bisi, A.; Masetti, M.; Gobbi, S.; Falchi, F.; Gentilomi, G. A.; Bonvicini, F.; Belluti, F. Alkyl Tail Variation on Chalcone-Based Quaternary Pyridinium Salts as Rule-of-Thumb for Antimicrobial Activity. *Arch. Pharm.* **2025**, *358* (5), No. e70003.
(26) Zavaroni, A.; Rigamonti, L.; Bisceglie, F.; Carcelli, M.; Pelosi, G.; Gentilomi, G. A.; Rogolino, D.; Bonvicini, F. Antimicrobial activity of Copper(II), Nickel(II) and Zinc(II) complexes with semicarbazone and thiosemicarbazone ligands derived from substituted salicylaldehydes. *Molecules* **2025**, *30* (11), No. 2329.
(27) Mali, S.; Vatagude, S. D.; Horitani, M.; Gurubasavaraj, P. M. Recent advances in Copper(II) Schiff base complexes: A comparative review of ligand core influence on biomedical applications. *J. Mol. Struct.* **2026**, *1360*, No. 145599.
(28) AlAjmi, M. F.; Hussain, A.; Rehman, M. T.; Khan, A. A.; Shaikh, P. A.; Khan, R. A. Design, Synthesis, and Biological Evaluation of Benzimidazole-Derived Biocompatible Copper(II) and Zinc(II) Complexes as Anticancer Chemotherapeutics. *Int. J. Mol. Sci.* **2018**, *19* (5), No. 1492.
(29) Sheldrick, G. M. SHELXT - Integrated space-group and crystal-structure determination. *Acta Crystallogr. A* **2015**, *71*, 3−8.
(30) Sheldrick, G. M. Crystal structure refinement with SHELXL. *Acta Crystallogr. C* **2015**, *71*, 3−8.
(31) Dolomanov, O. V.; Bourhis, L. J.; Gildea, R. J.; Howard, J. A. K.; Puschmann, H. OLEX2: a complete structure solution, refinement and analysis program. *J. Appl. Crystallogr.* **2009**, *42*, 339−341.
(32) GraphPad Software: San Diego, CA, USA.
(33) Repetto, G.; del Peso, A.; Zurita, J. Neutral red uptake assay for the estimation of cell viability/cytotoxicity. *Nat. Protoc.* **2008**, *3*, 1125−1131.

Downloaded from pubs.acs.org/acsodf/article-pdf/11/44/68833/6900612/acsomega.6c08107.pdf by UNIV DEGLI STUDI DI MODENA user on 17 November 2026

https://doi.org/10.1021/acsomega.6c08107
ACS Omega 2026, 11, 68833−68845